NOVA SCHOOL OF SCIENCE & TECHNOLOGY

DEPARTMENT OF PHYSICS

CATARINA SOFIA MIRANDA MATELA

BSc in Biomedical Engineering Sciences

PRODUCTION AND CHARACTERIZATION OF ANTIMICROBIAL AND ANTIOXIDANT SCAFFOLDS FOR SKIN TISSUE ENGINEERING

MASTER IN BIOMEDICAL ENGINEERING

NOVA University Lisbon

December, 2024

NOVA SCHOOL OF
SCIENCE & TECHNOLOGY

DEPARTMENT OF
PHYSICS

PRODUCTION AND CHARACTERIZATION OF ANTIMICROBIAL AND ANTIOXIDANT SCAFFOLDS FOR SKIN TISSUE ENGINEERING

CATARINA SOFIA MIRANDA MATELA

BSc in Biomedical Engineering Sciences

Adviser: Tânia Vieira
Researcher, NOVA University Lisbon

Co-adviser: Jorge Carvalho Silva
Associate Professor, NOVA University Lisbon

MASTER IN BIOMEDICAL ENGINEERING

NOVA University Lisbon
December, 2024

Production and characterization of antimicrobial and antioxidant scaffolds for skin tissue engineering

This document was created with the (pdf/Xe/Lua)LaTeX processor and the NOVAthesis template (v7.1.5) [1].

Acknowledgements

Começo estes agradecimento por expressar a minha profunda gratidão à pessoa sem a qual este trabalho não teria possível: a minha orientadora. Obrigada, Tânia, por me teres aceite neste projeto, por me teres ensinado todos os dias e por teres partilhado a tua abundante inteligência neste mundo da ciência, o teu olhômetro e o teu conhecimento em cultura portuguesa. A este legado familiar, à avó, filha e neta. A verdade é que podia escrever toda uma tese sobre a pessoa que és, sobre aquele dia que me deste a bolacha da Catarina, e sobre o facto de mereceres tudo de bom do mundo, mas fico-me pelo mais dos sinceros: obrigada orientadora de hoje e sempre.

Agradeço também ao meu orientador Professor Jorge Carvalho Silva. Obrigada por ter despertado este gosto por este tema, por me ter inscrito na cadeira de Engenharia de Células e Tecidos e por me ter apresentado o laboratório. Obrigada pela sua presença e apoio neste percurso de reta final de curso.

Ao laboratório que me acolheu este ano, um obrigada por me tornarem parte deste grupo incrivel. Sofia Sénior, Manuel, Alexandre, Filipa, Sofia Júnior, sem vocês isto tinha sido muito mais triste e díficil. De certeza que ainda não tinha gráficos na minha tese, não tinha ouvido Pedro Abrunhosa na renascença, não me tinha preparado para a defesa de tese com as mil perguntas mas também com as mil ajudas. Pelos lanchinhos, cafés, chocolates e gomas. Catarina, a minha co-co-orientadora, sem ti isto nem ia nem na metade. Nem sei o que escrever para ti, és um conjunto de risos e sabedoria única.Quero te escrever tanto mas primeiro, não tenho espaço e depois acho que nada seria digno da tua leitura, infelizmente esta parte não teve as tuas correções. A minha mãe do lab, a que mais aturou diretamente com a minha falta de jeito para ver as coisas que estão mesmo à minha frente. Quero ser delulu para sempre e continuar a pensar que um dia a familia vai se voltar a reunir para que todos os dias ao almoço haja o tal esperado chocolatinho e que haja gelo seco infinito. A vocês, um obrigado por esta experiência.

Imaginem acabarem um curso e não agradecer às pessoas que, sem elas, ainda tinha metade por acabar. Estes longos e, ao mesmo tempo, curtos 5 anos ao lado de Matildes (Maria e Catarina adicionais) definiram este meu percurso e esta experiencia. Carregamos isto com histórias, aulas a adivinhar o contexto do dia, testes, estudos na biblioteca,

churrascos e festas, cafés e quase férias nunca marcadas. A minha prova viva de que este curso nunca se faria sozinho. Ainda aguardo as nossas férias de finalistas. A vocês, Matildes, que me definiram como uma, gosto tanto de vocês.

Às minis que me acompanharam em tantas experiências, obrigada por cada momento que acreditaram em mim e que me puxaram para sair da minha zona de conforto. Sem dúvida alguma do melhor que a faculdade me deu.

À minha tão querida Associação, a que me acolheu e que me ensinou a palavra associativista. A todos os verdadeiros chefões que me fizeram crescer todos os dias, vocês têm o meu coração. Aos meus amados Gabinetes. Ao primeiro, não houve palavras, fomos e foi nossa, Rocha, Custódio, vocês foram tudo o que eu precisava e não sabia. Aos meus descendentes, JP e Madalena, vocês foram o toque de festa e cor à minha vida, que bom foi trabalhar com vocês.

Ao Homem que entrou bem a horas na minha vida e que me soube apoiar desde do dia que nos conhecemos. Acreditou mais que tudo nas minhas capacidades mesmo quando eu não o fazia. Esta última fase foi tão mais bonita ao teu lado, acolheste-me neste ultimo ano e tornaste-te no meu porto seguro. Ao meu cliché bunito, João Rocha, um obrigada gigante.

Não podia faltar o maior obrigada a quem me criou e esteve desde do dia 1. À minha família, que me apoiou incondicionalmente e se preocupou com o meu bem estar todos os dias desta etapa e da minha vida. A ti, avô, que me viste a iniciar isto e tenho a certeza que me vês a acabar, onde que que seja. A ti, avó, que me mimaste sempre e seres um porto de abrigo. Pelo amor de irmã que a Daniela me deu. Aos meus tios, irmãos, madrinha, por todo o amor envolvente. Pelo orgulho infinito de ser menina do papá. Pela minha melhor amiga ser a minha mãe e por me ter dado o apoio possível e ainda mais. Amo-vos a todos, e tudo isto é por vocês também.

A todos os que me acompanharam , apoiaram e moldaram, obrigada. Foi e sempre será, de corpo e alma.

”

“How lucky am I to have something that makes saying goodbye so hard”

— Winnie the Pooh

Abstract

Skin injuries present significant challenges in wound healing and tissue regeneration due to the complexity of their repair mechanisms. Chronic wounds, characterized by persistent inflammation and microbial infections, highlight the limitations of current skin substitutes, which frequently result in suboptimal regeneration and scar formation. This study develops multifunctional electrospun membranes composed of gelatin (GEL) and chitosan (CS) incorporating quercetin (Quer) and silver nanoparticles (AgNPs) to enhance wound healing. Membranes were produced via electrospinning and crosslinked with citric acid (CA) for improved stability. A Quer release assay revealed a biphasic release profile, with the 2.5% Quer membrane exhibiting the most controlled release after 24 hours, making it suitable for integration with AgNPs at a 1:200 (AgNPs:polymers) ratio. Four membranes were tested: CS-GEL, CS-GEL + Quer, CS-GEL + AgNPs, and CS-GEL + Quer + AgNPs. Scanning Electron Microscopy (SEM) with Energy Dispersive X-ray Spectroscopy (EDS) confirmed the incorporation of AgNPs. Observations suggested that quercetin interacts with AgNPs, potentially altering their release and performance. Inductively Coupled Plasma (ICP) analysis revealed a lower release of silver ions in the combined membrane. Cytotoxicity assays revealed slightly different results depending on the cell lines tested, with Human Neuroblastoma Cells (SH-SYS5) cells being the most sensitive. Notably, the CS-GEL + Quer + AgNPs membrane was viable in fibroblasts at concentrations as high as 7.5 mg/mL. While CS-GEL and CS-GEL + Quer demonstrated the best adhesion and proliferation over 11 days, CS-GEL + Quer achieved the highest antioxidant activity (>70%), but the combined CS-GEL + Quer + AgNPs membrane maintained a significant antioxidant activity similar to CS-GEL + Quer. Staining of fibroblast filaments and nuclei could prove the adhesion of cells to the membranes.

These results emphasize the potential of Quer and AgNPs collaboration in multifunctional membranes to address key challenges in wound healing, providing antioxidant, antibacterial, and regenerative benefits.

Keywords: Wound Healing, Quercetin, Silver Nanoparticles, Electrospun Membranes, Drug Release, Fibroblasts

Resumo

As lesões cutâneas apresentam desafios significativos na cicatrização e regeneração tecidual devido à complexidade dos seus mecanismos de reparação. As feridas crónicas, caracterizadas por inflamação persistente e infeções microbianas, evidenciam as limitações dos substitutos cutâneos atuais, que frequentemente resultam em regeneração subótima e formação de cicatrizes. Este estudo desenvolve membranas multifuncionais eletrofiadas compostas por gelatina e quitosano, incorporando quercetina e nanopartículas de prata (AgNPs), para melhorar a cicatrização de feridas.

As membranas foram produzidas por eletrofiação e reticuladas com ácido cítrico para melhorar a estabilidade. Os ensaios de libertação de quercetina revelaram um perfil de libertação bifásico, sendo a membrana com 2,5% de quercetina a que apresentou a libertação mais controlada ao fim de 24 horas, tornando-se a mais adequada para integração com AgNPs numa razão de 1:200 (AgNPs:polímeros). Foram testadas quatro membranas: CS-GEL, CS-GEL + Quer, CS-GEL + AgNPs e CS-GEL + Quer + AgNPs.

A análise de Microscopia Electrónica de Varrimento com Espectroscopia de Raios X por Dispersão de Energia (SEM-EDS) confirmou a incorporação de AgNPs. As observações sugeriram uma interação entre a quercetina e as AgNPs, que pode influenciar a libertação e o desempenho destes componentes. A análise de Plasma Indutivamente Acoplado (ICP) revelou uma menor libertação de iões de prata na membrana combinada. Os ensaios de citotoxicidade mostraram diferenças ligeiras entre linhas celulares, sendo as SH-SY5Y as mais sensíveis, enquanto a membrana CS-GEL + Quer + AgNPs foi viável em fibroblastos a concentrações de até 7,5 mg/mL.

Estas membranas demonstraram benefícios significativos na adesão e proliferação celular, com a CS-GEL + Quer a atingir a maior atividade antioxidante (>70%). A colaboração entre quercetina e AgNPs mostrou ser promissora para superar desafios na cicatrização de feridas, fornecendo propriedades antioxidantes, antibacterianas e regenerativas.

Palavras-chave: Cicatrização de Feridas, Quercetina, Nanopartículas de Prata, Membranas Eletrofiadas, Fibroblastos

Contents

List of Figures

List of Tables

Acronyms

AgNPs Silver Nanoparticles *(pp. xi, xii, xv, 2, 7, 8, 10–15, 18, 21–24, 26, 27, 29, 30, 32–34, 36, 37, 39, 40)*

CA Citric Acid *(pp. 6, 14, 24, 28, 29)*
CS Chitosan *(pp. xv, 2, 4, 6, 9, 10, 13, 21, 24, 25, 28, 39)*

DCFDA 2',7'-dichlorofluorescein diacetate *(pp. 18, 33)*
DLS Dynamic Light Scattering *(pp. 15, 26)*
DMSO Dimethyl Sulfoxide *(pp. 17, 18)*
DPPH 2,2-diphenyl-1-picrylhydrazyl *(pp. 17, 30)*

ECM Extracellular Matrix *(pp. 1, 4, 5)*

FTIR Fourier Transform Infrared Spectroscopy *(pp. 14, 15, 24)*

GEL Gelatin *(pp. xv, 2, 5, 6, 9, 10, 13, 21, 24, 25, 28, 39)*

HaCat Keratinocytes *(pp. 17, 31, 32)*
HFFF2 Human Caucasian Fetal Foreskin Fibroblast Cell Line *(pp. xv, 9, 17–19, 31–37)*

ICP Inductively Coupled Plasma *(pp. 16, 29)*
ICP-AES Inductively Coupled Plasma - Atomic Emission Spectrometer *(p. 16)*

PBS Phosphate-Buffered Saline *(pp. 16–19, 29, 30)*
PCL Polycaprolactone *(pp. 5, 10, 21)*
PDI Polydispersity Index *(p. 26)*
PEO Polyethylene Oxide *(pp. 5, 9, 13, 24)*
PVP Polyvinylpyrrolidone *(pp. 13, 33)*

Quer Quercetin *(pp. xv, 2, 7, 11, 12, 14–18, 21–34, 36, 39)*

ROS Reactive Oxygen Species *(pp. 1, 18, 33, 34, 39)*

SEM Scanning Electron Microscopy *(pp. xv, 14, 21, 23, 29)*

1

Introduction

1.1 Context and Motivation

The skin, as the body's primary physical barrier, plays a vital role in protecting against external environmental threats such as microbial invasion, mechanical damage, and harmful chemicals. Its structure comprises three layers: the epidermis, dermis, and hypodermis, with the first two being the primary focus of tissue engineering due to their importance in barrier function and wound healing [2].

The epidermis, the skin's outermost and thinnest layer, consists primarily of keratinocytes and lacks blood vessels, while the dermis contains fibroblasts responsible for producing type I collagen, a critical Extracellular Matrix (ECM) component. When injuries occur, the skin's ability to heal effectively depends on the coordination of these layers. However, in chronic wounds—such as diabetic ulcers or venous leg ulcers—the healing process is disrupted, leading to a prolonged inflammatory state and impaired regeneration. Persistent inflammation in chronic wounds is driven by microbial infections and excessive Reactive Oxygen Species (ROS), creating a cycle of oxidative stress that exacerbates tissue damage and delays healing. High ROS levels, while beneficial in moderation for angiogenesis and pathogen defense, cause cellular damage and apoptosis when uncontrolled, further disrupting ECM remodeling and prolonging the inflammatory state. These challenges underscore the need for innovative tissue engineering strategies to mitigate inflammation, regulate ROS, and promote effective regeneration [2, 3].

Skin tissue engineering emerges as a promising approach to overcome the limitations inherent in current wound healing strategies. By harnessing the synergies of biomaterials, bioactive molecules, and cells, tissue engineering intends to craft scaffolds with the capacity to facilitate comprehensive tissue reconstruction. Researchers have extensively explored a spectrum of materials, encompassing natural and synthetic polymers, proteins, lipids, and diverse scaffold architectures, including hydrogels, fibers, particles, and sponges. This research area aims to develop scaffolds that not only promote wound healing but also prevent infections, addressing the skin's inherent limitations in preventing infections or regulating temperature in cases of severe wounds. Nevertheless, the complexity of

the wound healing process and the need for long-term solutions demand innovative approaches [4].

The current landscape of skin tissue engineering grapples with challenges in providing effective solutions for extensive skin injuries affecting both the epidermal and dermal layers. Despite the availability of commercial skin substitutes, persistent limitations, including the risk of not achieving complete regeneration of the layers and structures within the dermis, hinder their success. Additionally, challenges extend to inadequate innervation within scar tissue, exacerbating skin conditions due to the insufficient restoration of damaged skin tissue. Notably, severe scars resulting from the closure process of extended and deep skin wounds remain a significant concern. High contracture, loss of sensitivity, poor pigmentation, and the disappearance of cutaneous adnexa (hair follicles and sweat glands) are common features of restored skin. These issues contribute to significant morbidity and aesthetic concerns, emphasizing the urgent need for the development of more effective bioengineered skin models that foster regeneration rather than mere repair [5, 6].

1.2 Objectives

This project aims to develop innovative membrane for wound healing by integrating key components that address critical challenges associated with chronic wounds, such as prolonged inflammation and microbial infections. The strategy involves combining natural polymers — GEL and CS — with bioactive compounds, specifically Quer as an antioxidant flavonoid already recognized for its role in wound healing, and AgNPs, well-known for their strong antibacterial properties. The primary objectives of this research include:

- Achieving antimicrobial and antioxidant properties by incorporating AgNPs and Quer into the membranes.
- Achieving a controlled drug delivery from the membranes, focusing on the sustained release of Quer, to address concerns related to systemic toxicity and ensure an optimal drug concentration at the wound site.
- Investigate and promote cellular proliferation and adhesion on the developed scaffold through *in vitro* analysis, emphasizing the enhancement of cell-scaffold interaction.

By achieving these objectives, this research aims to contribute significantly to the field of wound healing strategies, offering a multifaceted approach to scaffold development that emphasizes antimicrobial efficacy, antioxidant qualities, and improved cellular interactions.

2

Theoretical Concepts

2.1 Electrospinning

Electrospinning stands out as a versatile technique harnessing electrostatic forces to craft fibers, typically ranging from nanometers to micrometers. This intricate process involves a high-voltage power supply, a syringe equipped with a capillary needle or spinneret, a syringe pump and a grounded collector, often a metal plate or rotating mandrel, which influences the uniformity of fiber distribution. Subjecting a polymeric solution to high voltages results in a charged jet, where electrostatic repulsion and surface tension cause instabilities, leading to jet elongation and nanofiber formation. A schematic representation of the electrospinning process is shown in Figure 2.1. Achieving meticulous control over the diameter and morphology of these fibers involves precise adjustments in various parameters. Factors stemming from the solution, such as polymer concentration, viscosity, and conductivity, play a pivotal role. Additionally, parameters directly related to the electrospinning process, including applied voltage, distance from the needle tip to the collector and flow rate, contribute to this control. It is important to note that environmental conditions (temperature and humidity) can also exert influence over the creation of these fibers [7, 8].

Fiber elongation is primarily driven by repulsive Coulombic electrostatic forces, alongside viscoelastic forces and surface tension, shaping fibers during electrospinning. Achieving a delicate balance between feed rate and electrostatic extraction rate is crucial. The process progresses through phases, including the formation of a hyperbolic conical shape (Taylor cone), jet eruption, linear flow, and eventual nanofiber production. The rapid whipping motion of the jet facilitates solvent evaporation, leaving primarily dried polymer fibers to be deposited into the collector. Additionally, the distance from the tip to the collector must be sufficient to allow complete solvent evaporation before the fibers reach the collector; if the distance is too short or too long, non uniform fibers may result. The optimal distance depends on factors such as polymer solution concentration and applied voltage [9, 10].

In the context of wound healing, electrospun fibers provide advantages like increased

adaptability, encapsulation and delivery of biopharmaceuticals, gas exchange with the wound environment, absorption of wound exudates, and surface functionalization for enhanced biocompatibility and wound management [8]. Despite versatility, challenges persist, necessitating careful control of parameters [8].

These nanofibers, mimicking the Extracellular Matrix (ECM), find applications in wound healing, offering adaptability, controlled drug release, and support for cellular processes. This makes them powerful tools in tissue engineering and regenerative medicine [7, 8].

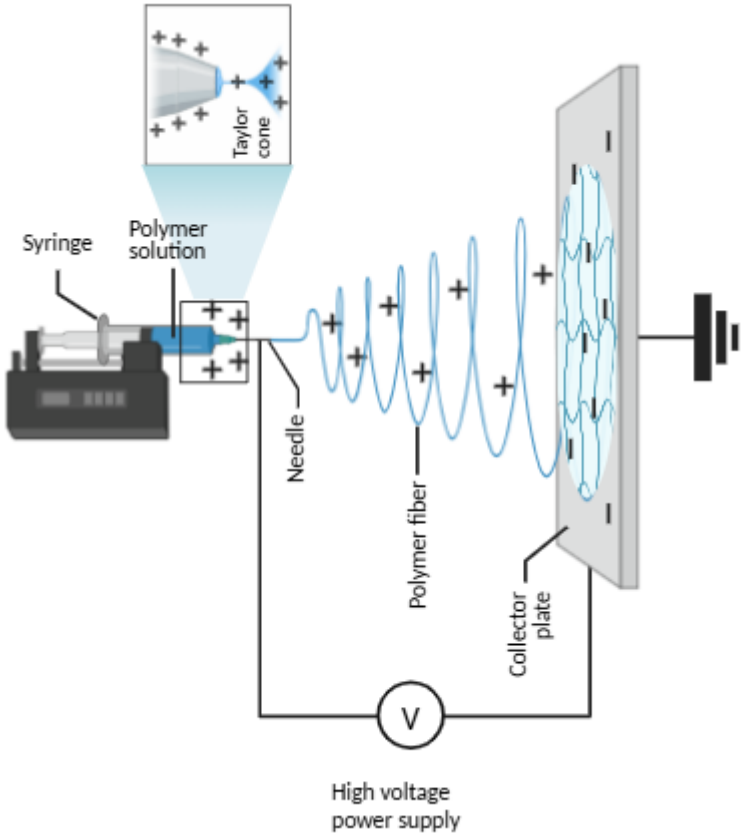

Figure 2.1: Schematic of a electrospinning setup. Created from *BioRender*.

2.2 Polymers

2.2.1 Chitosan

Chitosan (CS), derived from the partial or full deacetylation of chitin, a prevalent natural polysaccharide, has garnered significant attention for its biocompatibility, biodegradability, and antibacterial properties. Notably, chitosan uniquely possesses a positive charge among natural alkaline polysaccharides, making it one of the most abundant natural polysaccharides. Nevertheless, the electrospinnability of chitosan is hindered by its polycationic nature and chemically rigid structure, stemming from its functional groups

(Figure 2.2). This results in the production of solutions with high viscosity and electrical conductivity, posing significant obstacles to the electrospinning of chitosan. A solution to this challenge involves blending chitosan with compatible polymers like Polyethylene Oxide (PEO) and Polycaprolactone (PCL). This strategic combination effectively overcomes the inherent limitations, resulting in fibers with an expansive surface area and porosity similar to the ECM — qualities highly advantageous for wound healing applications. Despite these promising attributes, drawbacks include compromised wet stability and suboptimal mechanical properties in aqueous environments, posing constraints in tissue engineering applications. However, electrospun chitosan serves as a scaffold with unique features such as wound adhesion, absorption, oxygen permeability, and resorbability [11, 12].

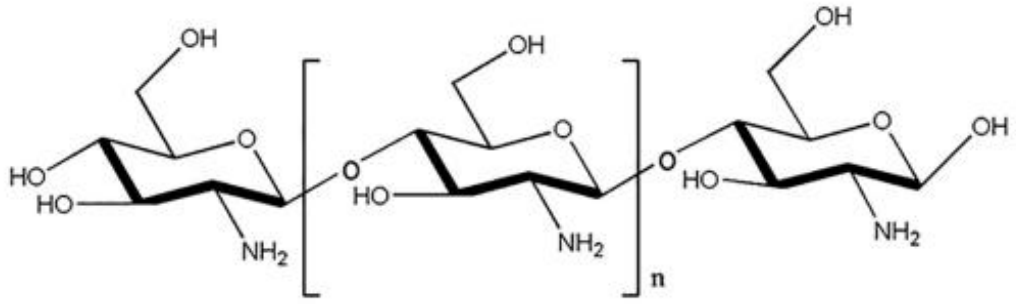

Figure 2.2: Chemical Struture of Chitosan. Retrieved from [13].

2.2.2 Gelatin

Gelatin (GEL), a denatured protein primarily derived from collagen through alkaline and acid hydrolysis, mirrors one of the primary components of the extracellular matrix. It serves as a natural polymer renowned for its biocompatibility, biodegradability, and low toxicity. These attributes make gelatin conducive to promoting cell interactions, fostering adhesion, differentiation, and proliferation. Possessing both positive and negative electrical charges – Figure 2.3 - allows gelatin to undergo diverse chemical modifications, proving valuable in developing targeted drug release systems. Despite these advantages, gelatin's stability is a difficulty since it dissolves easily in water and lacks structural integrity. To overcome this limitation, crosslinking is essential [14, 15]. Fish gelatin, specifically derived from the partial hydrolysis of collagen in fish skin, has emerged as a promising alternative to mammalian-derived gelatin. Compared to porcine and bovine gelatin, fish gelatin contains lower levels of proline and hydroxyproline, resulting in reduced thermal stability and mechanical properties. Despite these limitations, fish gelatin is increasingly valued due to the abundant availability of fish skin as a by-product of the fish-processing industry. Its recovery not only reduces industrial waste but also supports economic sustainability, positioning fish gelatin as an excellent candidate for tissue engineering

studies while addressing public health concerns and religious restrictions associated with mammalian sources [16].

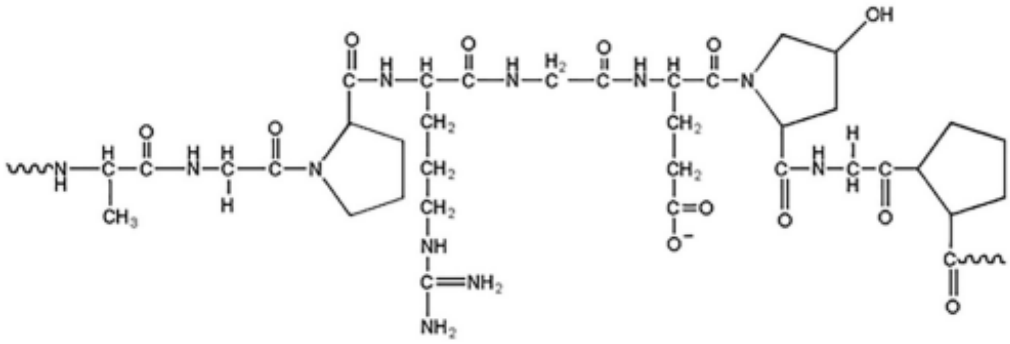

Figure 2.3: Chemical Struture of Gelatin. Retrieved from [13].

2.3 Crosslinking Agents

CS and GEL are widely used natural polymers in nanofiber fabrication due to their biocompatibility and biodegradability. However, both materials are highly hydrophilic, causing nanofibers produced from CS and GEL to lose their fibrous morphology when in contact with aqueous environments. This limitation necessitates the use of crosslinking treatments to enhance the water stability of these membranes, ensuring their structural integrity and functionality in biomedical and other applications [17].

2.3.1 Citric Acid

Citric Acid (CA) is increasingly utilized as a cross-linking agent, leveraging its natural cross-linking properties and non-toxic nature. With three carboxyl groups, of which two are reactive, CA interacts with the amino groups of gelatin, potentially forming imide and amide structures (Figure 2.3). While CA enhances water resistance and mechanical properties, an excess may increase hydrophilicity and solubility, underscoring the importance of tailored formulations based on specific material requirements. This agent exhibits a dose-dependent improvement in tensile strength of gelatin films, indicating significant interactions with gelatin [14, 18]. Its versatility extends to chitosan nanofibers, where CA enhances solvent resistance and mechanical properties. In chitosan membranes, CA forms carboxyl-amine groups, showcasing its role in crosslinking [19]. As these interactions are ionic, their utility is hindered by inherent challenges, including limited stability and a significant reliance on environmental conditions, such as pH [20]. Overall, CA emerges as a non-toxic, cost-effective crosslinker with diverse applications in enhancing material characteristics.

2.4 Quercetin

Quercetin (Quer) a flavonoid, is extensively utilized for managing metabolic and inflammatory disorders. Abundantly present in fruits, vegetables, and seeds, it imparts a range of health benefits, encompassing antifibrotic and anticancer properties, along with immunomodulation. Its unique capacity to modulate inflammation, combined with antioxidant and antibacterial features, is noteworthy [21]. Its structure, as shown in Figure 2.4, characterized by multiple hydroxyl (-OH) groups and a carbonyl group, enables it to chelate metal ions and efficiently neutralize free radicals, contributing to its well-established antioxidant properties [22]. Despite its promising therapeutic properties, quercetin faces several challenges that hinder its clinical application. The main drawbacks include poor aqueous solubility, a short metabolic half-life, and potential toxicity. These limitations affect its effective delivery, absorption, and bioavailability, ultimately reducing its overall pharmacological impact. However, when conjugated with certain nanomaterials in drug delivery systems, Quer's bioavailability can be enhanced, potentially minimizing adverse effects and toxicity [23].

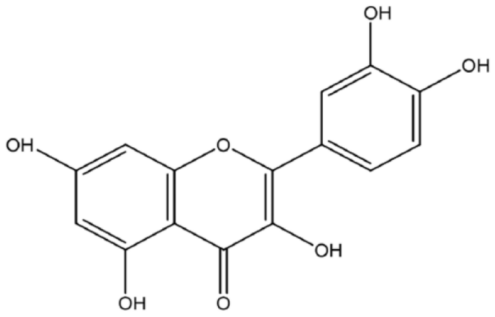

Figure 2.4: Chemical Struture of Quercetin. Retrieved from [24].

2.5 Silver Nanoparticles

Silver Nanoparticles (AgNPs), known for their high electrical conductivity, antimicrobial properties that can prevent the emergence of antibiotic resistant bacteria, chemical stability, and catalytic potential, have garnered significant interest. These nanoparticles can be incorporated into biocompatible materials with precisely controlled properties, making them a sustainable and effective option for antibacterial applications, particularly in fields like biomedicine, including wound healing. Moreover, their synthesis aligns with environmentally friendly and cost-effective approaches [25]. These nanomaterials play a pivotal role in advancing wound healing by virtue of their intrinsic properties, including antimicrobial, anti-inflammatory, and antioxidant effects, fostering enhanced cell proliferation and skin remodeling. Furthermore, AgNPs serve as effective carriers for drug delivery, augmenting the efficiency of wound treatment. Beyond wound healing, AgNPs find applications in medicines, and controlling microbial growth in biological systems [25, 26]. The synthesis of AgNPs encompasses various methods—chemical, physical, and

biological—each presenting distinct advantages and limitations. Despite their widespread applications, challenges such as significant energy consumption in certain synthesis methods and the dose-dependent toxicological effects persist [27]. In summary, AgNPs emerge as versatile nanomaterials with diverse applications, particularly in antibacterial and wound healing strategies.

3

State of the Art

3.1 Electrospun Membranes

Natural polymers, including collagen, gelatin, fibrin, keratin, and chitosan, have become increasingly popular in scaffold design. These materials offer inherent biocompatibility, cell adhesion motifs, and controlled degradation *in vivo*. Techniques such as self-assembly, chemical crosslinking, freeze-drying, and electrospinning are employed to create porous and soft substrates that mimic the dermis and epidermis, promoting cell migration and future vascular infiltration. With the production of membranes using the techniques outlined, natural polymers are employed to prevent wound infections [2, 28].

Many researchers have investigated electrospinning nanofibers incorporating GEL and CS in varying proportions to optimize their properties. Vafania et al. (2019) fabricated nanofibers with different GEL/CS ratios (1:6, 1:8, and 1:10), determining that the 1:6 ratio provided optimal results in terms of stability and achieving a uniform fiber diameter [29]. Similarly, Fathi et al. (2019) produced CS-GEL nanofibers by varying the CS/GEL ratios and observed that an increase in CS content resulted in the formation of finer nanofibers with smaller diameters and improved thermal resistance compared to the individual components. The most favorable results were obtained with a 1:4 CS/GEL ratio under an applied voltage of 17 kV, highlighting the influence of solution composition and processing parameters on fiber morphology [30].

In a subsequent study in 2015, following the production of nanofibers comprising polycaprolactone, CS, and GEL [31], S. Gomes et al. (2017) advanced their research by creating membranes through the electrospinning of polymeric blends formulated with these polymers, particularly GEL sourced from cold water fish skin. The GEL-based scaffolds were crosslinked using glutaraldehyde vapor. In addition to physiochemical analyses, the scaffolds underwent *in vitro* examination with Human Caucasian Fetal Foreskin Fibroblast Cell Line (HFFF2) to assess their suitability for skin tissue engineering. The CS/GEL solution in this study comprised 2% CS and 2% GEL , with the inclusion of a small percentage of PEO. This addition aims to address challenges related to electrospinning CS-containing solutions, attributed to its cationic nature and high conductivity. Concerning *in vitro* cell

adhesion, the CS/GEL scaffolds demonstrated the second-best results outperformed by the GEL and PCL mixtures [32].

3.2 Role of AgNPs

Some of the available options for treating skin wounds have difficulty in effectively combating infections and inflammation. Especially in cases of severe injuries, such as deep burns, where there is fluid loss and bacterial contamination, the outcomes can be serious. Additionally, the presence of exudates between the wound and the dressing can exacerbate infection and inflammation, delaying natural healing. Thus, developing a wound healing scaffold with antibacterial properties becomes essential to address this common issue [28].

Additionally, these scaffolds are designed to possess properties that can accelerate wound healing, including anti-inflammatory and anti-microbial features. The incorporation of nanoparticles into membranes, particularly AgNPs, has garnered significant attention for its potential in wound healing. As discussed in the following section, AgNPs offer distinct advantages that contribute to enhancing the wound healing process [33]. Numerous studies have investigated AgNPs, revealing enhanced antimicrobial activity *in vitro* and accelerated wound healing in mice *in vivo*. Furthermore, these nanoparticles have exhibited the ability to stimulate cell migration when cultured with fibroblasts [28].

Ganesh et al. (2016) developed electrospun fibers using polyvinyl alcohol and CS, co-encapsulated with AgNPs to achieve a synergistic wound-healing effect. The silver was incorporated in the form of silver nitrate at a ratio of 10 w/w %. Furthermore, formic acid was employed as a reducing agent to generate colloidal AgNPs within the composite polymeric solution, along with the active agent sulfanilamide. *In vitro* studies indicated an initial rapid release followed by sustained and slower release from the composite nanofibers. Antibacterial evaluations demonstrated a significant increase in the zone of inhibition against common pathogens, such as *Staphylococcus aureus*, *Escherichia coli*, and *Pseudomonas aeruginosa*, in PVA–CS nanofibers loaded with AgNPs and sulfanilamide compared to plain nanofibers, thus highlighting a notable enhancement in the antimicrobial effects of the composite membranes [34].

Another study, led by F. Yang et al. (2019), also utilized electrospun membranes of CS with AgNPs. Chitosan-based membranes were loaded with AgNPs at concentrations of 0 % (control), 1 % (Ag1), and 5 % (Ag5) w/w. The research uncovered sustained silver ion release for up to 28 days *in vitro*. In a rat subcutaneous model, AgNPs incorporation exhibited potent, dose-dependent antibacterial effects, with the Ag5 group achieving sustained bacterial reduction to zero after 7 days. In a rat skin model, AgNPs did not impede wound healing rates; instead, they accelerated closure in the Ag1 and Ag5 groups, suggesting a synergistic effect between CS and AgNPs. These studies collectively emphasize the promising potential of nanofibrous materials with AgNPs for enhanced wound healing applications [35].

3.3 Quercetin

Recent advances in electrospinning allow the fabrication of membranes, valued for their narrow diameter and porous structure as described earlier. These membranes serve as effective delivery systems for biomolecules, genes, and drugs due to their high specific surface area. Notably, electrospun membranes, with their substantial surface area-to-volume ratios, play a crucial role in topical drug delivery, exploiting the skin's extensive surface area. These membranes, capable of delivering both hydrophilic and hydrophobic drugs, find applications in wound dressings, contributing to advanced drug-releasing wound treatment technologies [36, 37].

Efforts to overcome the challenges mentioned in the previous section have prompted exploration into various drug delivery systems. Strategies, including encapsulation in nanomaterials, seek to enhance the bioavailability of Quer while simultaneously mitigating its potential toxicity [23].

Several studies have explored the use of Quer in nanofibers and nanoparticles to create a controlled drug delivery system, aiming to mitigate toxicity risks. The antioxidant properties of Quer also contribute to accelerating the healing process. Some of these studies are summarized in Table 3.1, including the mass percentage of Quer used and the main outcomes reported.

Table 3.1: Results and Characteristics of the Use of Quercetin for Wound Healing in the Literature.

References	**Wound Dressing Materials**	**% Quercetin**	***In vitro*/*In vivo* Models**	**Main Outcomes**
G. Ajmal, et al. (2019) [38]	PCL-GEL nanofibers	5% w/w of polymers	*S. aureus*/Wistar rats	Accelerated wound healing in the scaffold treated with quercetin: Complete closure of wounds in 16 days.
A. Choudhary, et al. (2020) [39]	Chitosan tripolyphosphate nanoparticles	0.3%, 0.1%, 0.03% w/v	Wistar rats	Quercetin nanoparticles (0.03%) exhibited a better anti-inflammatory effect and also a better wound healing.
L. Zhou, L. Cai, H. Ruan, et al. (2021) [40]	Chitosan Oligosaccharide/PCL nanofibers	5% w/w relative to PCL	*E. coli* and *S. aureus*	The fibers containing quercetin maintained a long-term bacteriostatic effect, potentially beneficial for wound dressing.
S.K. Karuppannan, et al. (2022) [41]	Electrospun nanofibers PCL/GEL	5% w/w	3T3 fibroblasts/Wistar rats	On scaffolds containing quercetin, there was an increase in cell density and a reduction in the time required for complete epithelization.

The combination of Quer and AgNPs in wound healing remains a relatively understudied area, but recent research highlights its potential. One study developed a hydrogel using

Carbopol 934 as the synthetic polymer and aloe vera as an additional component. The hydrogel, containing quercetin-loaded AgNPs, demonstrated its effectiveness in treating diabetic wounds. The hydrogel showed strong antimicrobial activity against *S. aureus* and *E. coli* and significantly accelerated wound closure and re-epithelialization in an *in vivo* diabetic wound model. These results suggest that the synergistic effects of quercetin and AgNPs could provide a valuable solution for enhancing wound healing outcomes [42].

Another study explored quercetin-assisted silver nanoparticles (Quer-AgNPs), synthesizing them under optimized conditions with a spherical morphology and average size of 20 ± 3.6 nm. These nanoparticles demonstrated strong antioxidant and anti-inflammatory properties, along with effective antimicrobial activity, particularly against *S. aureus* and *E. coli*. Additionally, Quer-AgNPs exhibited high blood compatibility, with minimal hemolysis at concentrations up to 500 μg/mL. These findings underscore the potential of Quer-AgNPs as a multifunctional solution for wound healing and other biomedical applications [22].

4

Experimental Procedure

4.1 Production of Silver Nanoparticles

AgNPs were synthesized using a protocol already optimized in the laboratory [43]. Polyvinylpyrrolidone (PVP), silver nitrate, and sodium borohydride ($NaBH_4$) were used. A solution of PVP 1 % in 5 mL of distilled water was prepared and stirred. Following that, a solution of silver nitrate at a concentration of 29.50 mM in 500 µL of water was added to the PVP solution while stirring, and then the mixture was placed in an ice bath. In another eppendorf, 29.50 mM of $NaBH_4$ were dissolved in 500 µL of water and kept in an ice bath. The stirring of the silver-PVP solution was intensified, and the $NaBH_4$ solution was added dropwise. The resulting mixture was stirred vigorously and kept in the ice bath for 30 minutes. After obtaining the final solution, the nanoparticles were dialyzed using cellulose dialysis tubing membranes (Sigma, molecular weight cut-off = 14,000 Dalton) for 3–4 days, changing the water twice daily, to remove any unreacted precursors, solvents, or by-products, ensuring the purity of the nanoparticle solution.

4.2 Production of Membranes

The membrane production process followed a method similar to that developed by the Tissue Engineering Group [32], employing CS and GEL as natural polymers and the electrospinning technique. To prepare the solution for electrospinning, 2 wt % of GEL (water fish skin – Sigma), 2 wt % of CS (Cognis, Mw = 500 kDa and degree of deacetylation = 75.5 %), and 0.2 wt % of PEO (Sigma, Mv = 2,000,000) were dissolved in 90:10 acetic acid (Fluka): distilled water and were magnetic stirred overnight. For the electrospinning procedure, the solution was placed in a 5 mL plastic syringe connected to a 21G needle tip, which as placed in a syringe pump with a 0.30 mL/h flow rate. The collector cover with aluminum foil and ground connected was place 25 cm away from the needle tip. A high voltage power supply was connected to the needle tip and a voltage ranged between 15 V and 18 V was applied. The temperature and humidity during membrane production were maintained at 20–22 °C and 40–58 %, respectively. The resulting membrane was left

to dry for 48h.

In addition to the polymeric standard solution, Quer and AgNPs were incorporated at different concentrations to produce various membranes. The compositions included:

- Membranes with quercetin (Sigma-Aldrich) at three different concentrations: 1.25 %, 2.5 %, and 5 % (w/w of the total polymer mass).
- Membranes containing AgNPs at a concentration of 1:200 (v/v dilution) [44].
- A hybrid membrane incorporating both components: 2.5 % quercetin and 1:200 AgNPs.

After evaluating the initial three Quer concentrations, 2.5 % Quer was selected as the optimal concentration for subsequent experiments. Therefore, the assays following drug release were performed using the four resulting membranes: CS-GEL, CS-GEL + Quer, CS-GEL + AgNPs, and CS-GEL + Quer + AgNPs, with the membrane containing Quer specifically referring to the 2.5 % concentration.

These solutions were stirred for 30 minutes prior to electrospinning to ensure dispersity, and the electrospinning parameters remain the same of the standard polymeric solution. CA (Sigma-Aldrich), at 30 % of the total polymer weight, was added to the prepared solutions before electrospinning for subsequent crosslinking. The crosslinking process involved a heat treatment, where the membranes were first placed in an oven at 100 °C for 12 hours, followed by 170 °C for 3 hours [19].

4.3 Characterization of Membranes

To assess the morphology of the membranes and confirm their physical properties, various assays were performed. One such process involves Scanning Electron Microscopy (SEM) to study membrane morphology, Fourier Transform Infrared Spectroscopy (FTIR) for molecular analysis and chemical bonding and evaluation of swelling in different buffers.

4.3.1 Scanning Electron Microscopy

SEM allows the visualization of the nanoscale structure of the produced membranes. The membrane's morphology was evaluated using the TM3030 Plus Hitachi Tabletop Microscope, and the resulting images were used to measure the average diameters of the fibers of each membrane type. To prepare the samples for SEM, these were cut into small rectangles and placed on a double-side carbon tape and then coated with 35 nm layer of gold: palladium (60:40). To observe the AgNPs in the fibers, membranes without coating were observed using the ultra-high-resolution scanning electron microscope Hitachi SEM regulus 8220 equipped with energy dispersive -ray spectroscopy (EDS). The images were acquired in backscattered mode and the elemental analysis of Ag, C and O elements in the membranes was also evaluated by the EDS analysis (Appendix A). To determine the

average diameter of each fiber, the *ImageJ* software (National Institute of Health, USA) was utilized to measure approximately 70 fiber segments, considering the scale of the acquired images. Subsequently, the mean diameter and standard deviation were calculated [45].

4.3.2 Fourier-Transfrom Infrared Spectroscopy

To assess the types of molecular interactions that occurred between the components within the membranes, FTIR analysis was conducted. This analysis was performed using a Perkin-Elmer Spectrum Two FTIR in ATR mode (attenuated total reflectance). The resulting transmittance spectrum covered a wavenumber range from 4000 cm^{-1} to 400 cm^{-1}.

4.4 Characterization of Silver Nanoparticles

4.4.1 Dynamic Light Scattering and UV-Vis Spectrophotometry

To confirm the successful production of AgNPs, these were characterized by UV-Vis Spectrophotometry with a Sarspec RES+ spectrophotometer, to observe the surface plasmon resonance (SPR) of AgNPs. To measure the size of the synthesized AgNPs, Dynamic Light Scattering (DLS) was performed. DLS utilizes the principle of Brownian motion to determine the size of the particles. The diameter measured in this process is derived from the way the particles diffuse in a certain solvent, which in this case was water for the AgNPs. The sample analyzed had a concentration of 100 µg/mL and was measured five times using a cuvette at a scattering angle of 90 °. The DLS data were obtained using the SZ-100 nanoparticle series from Horiba Lda with a laser of 532 nm. The data were analyzed with Excel Solver, applying the Stokes-Einstein equation and correlation functions, explained with more detail in Appendix B [46, 47].

4.5 Quercetin Calibration Curve and Encapsulation Efficiency

A calibration curve was generated by measuring the absorbance of Quer solutions at different concentrations. This calibration curve is essential for the subsequent encapsulation and release assays of Quer, with absorbance measurements consistently taken at a wavelength of 376 nm [42]. The concentrations used to build the calibration curve were 5 µg/mL, 10 µg/mL, 15 µg/mL, 20 µg/mL, and 25 µg/mL (Appendix D). 5 mg of un-crosslinked Quer-loaded membranes were dissolved in 5 mL of water with 100 uL of acetic acid. The control sample, consisting of CS-GEL fibers, was prepared similarly for UV-Visible spectrophotometer absorbance measurements. The encapsulation efficiency (EE) was calculated using the Equation 4.1:

$$EE(\%) = \frac{\text{Actual Quantity of Quercetin in the Fibers}}{\text{Theoretical Quantity of Quercetin in the Fibers}} \times 100 \tag{4.1}$$

4.6 Drug Release Assay

4.6.1 Quercetin Release

The release assay was performed with membranes containing different concentrations of Quer – 1.25 %, 2.5 %, and 5 % – to analyze the Quer release profile and how its concentration affects the release in different buffers. The assay was performed in triplicate using three different buffers: Phosphate-Buffered Saline (PBS) 1x (pH 7.4), a simulated wound fluid solution (pH 8) to mimic skin wound conditions and a buffer to simulate normal skin conditions (pH 5.6). The simulated wound fluid solution was prepared by adding 0.68 g of NaCl, 0.22 g of KCl, 0.35 g of NaH_2PO_4 and 2.50 g of $NaHCO_3$ to 100 mL of water, which results in a solution with a pH 8 [48]. To mimic normal skin conditions, the solution was prepared by adding 7.72 g of sodium acetate and 352.50 mg of acetic acid to 1 L of water [49].

All these solutions contained 0.02 % (v/v) Tween-80 to facilitate the release of Quer from the membranes, due to its low solubility in aqueous solutions. Quer release was carried out by incubating the membranes in 8 mL of each buffer at 37 °C, with a constant agitation of 100 rpm. At each time point, 2 mL of the solution was withdrawn to measure absorbance at 376 nm using a Sarspec RES+ UV-Vis spectrophotometer. The steps for calculating the cumulative mass release are detailed in Appendix E. The withdrawn samples were discarded, and 2 mL of fresh buffer was added to maintain the total volume. The reference sample was prepared in the same way, using the standard membrane without Quer, and the buffers were changed at each time point just like the samples containing Quer.

4.6.2 Inductively Coupled Plasma – Atomic Emission Spectrometer

To evaluate the amount of silver ions released from the membranes containing these particles, Inductively Coupled Plasma - Atomic Emission Spectrometer (ICP-AES) assays were conducted. For sample preparation, a release assay was performed by immersing 5 mg of membrane in 8 mL of PBS with 0.02 % (v/v) Tween-80, similarly to the Quer release environment. The samples were prepared in triplicates and collected at 6 and 24 hours of incubation. The tubes were agitated at 100 rpm at 37 °C. After the specified time, 2 mL of the solution were filtered using a 0.22 µm pore-size filter to remove fiber residues and then transferred to an eppendorf tube. PBS with 0.02 % Tween-80 was used as the reference for ICP-AES analysis. The ICP-AES analysis was conducted using a Horiba Jobin-Yvon, France, Ultima model, equipped with a 40.68 MHz RF generator, Czerny-Turner monochromator (1.00 m sequential), and an AS500 autosampler. Data acquisition and processing were performed using Inductively Coupled Plasma (ICP) Analyst software version 5.4.2.

4.7 Antioxidant Activity

4.7.1 2,2-Diphenyl-1-picrylhydrazyl Radical Scavenging Assay (DPPH)

To evaluate the antioxidant activity of the membranes, a 2,2-diphenyl-1-picrylhydrazyl (DPPH) assay was performed. For comparative analysis between different membranes types, 5 mg of each membrane were weighed and immersed in 3 mL of a 100 µM DPPH (Aldrich) solution. The membranes for this study were CS-GEL, CS-GEL + Quer, CS-GEL + AgNPs and CS-GEL + Quer + AgNPs. Additionally, the antioxidant activity of pure Quer at a concentration of 0.25 mg/mL was assessed under identical conditions. The solutions were protected from light and agitated at 100 rpm for one hour. DPPH assay was also conducted at different time points to assess the antioxidant activity overtime from Quer-containing membranes. For this purpose, 5 mg of membrane was incubated in 2 mL of PBS (1x) containing 0.02 % Tween-80 for 1, 3 and 6 hours. After incubation, the solution containing the membranes was mixed with 1 mL of the DPPH solution and left to react for 30 minutes under the same conditions. The antioxidant activity of the DPPH solutions was quantified using Sarspec RES+ UV-Vis spectrophotometer at 517 nm. The percentage of antioxidant activity was calculated using the Equation 4.2:

$$EE(\%) = \frac{\text{1 - Sample}}{\text{Control}} \times 100 \tag{4.2}$$

4.8 *In Vitro* Characterization

4.8.1 Cytotoxicity Assays

The potential cytotoxicity of Quer and the produced membranes was evaluated using different cell types: ?? (ATCC CRL-2266 ™), HFFF2 (ECACC 86031405), and Keratinocytes (HaCat) (Addexbio (San Diego, CA, USA)). Various cytotoxicity assays were conducted, including direct methods, using pure Quer and indirect methods, using membrane extracts. These extracts were sterilized before culturing by placing them in an oven at 120 °C for 2 hours.

For each assay, cells were initially seeded in a 96-well plate at a density of 30,000 cells/cm², except for HFFF2, which were seeded at 25,000 cells/cm² due to their larger size and greater surface area occupancy. The cells were incubated for 24 hours in either low glucose Dulbecco's Modified Eagle's Medium (DMEM-LG, Biowest) for HFFF2 and ??, or high glucose Dulbecco's Modified Eagle's Medium (DMEM-HG, Biowest) for HaCat cells, with both media supplemented with 10 % fetal bovine serum (FBS, Biowest) and 1 % penicillin-streptomycin (P/S, Gibco). In the direct method, after the 24-hour incubation, the medium was replaced with one containing 500 μM of Quer and 0.2 % Dimethyl Sulfoxide (DMSO), followed by a series of 1:2 dilutions, with four replicates per group. This assay was conducted with the three previously mentioned cell lines.

A cytotoxicity assay was also conducted to evaluate the potential cytotoxicity of membranes containing Quer and/or AgNPs. The protocol followed was similar to the one previously described, exposing the cells to the membrane extracts that were produced over a 24-hour period. Cells were seeded in a 96-well plate and incubated as described before. The experiment began with a concentration of 15 mg/mL, followed by successive 1:2 dilutions. All assays included two control groups: a negative control with fresh medium only, and a positive control with 10 % of DMSO added to fresh medium. The pure Quer assay also included a DMSO solvent control with 0.2 % DMSO. The plates were incubated for 48 hours in an MCO-19AIC(UV) CO_2 incubator at 37 °C, in a humidified atmosphere with 5 % CO_2. Cell viability was assessed using a resazurin (Alfa Aesar) assay. Detailed procedures for cell culture and the resazurin assay are provided in Appendix C. The samples were normalized to the negative control, and the results were expressed as *mean ± combined standard uncertainty*.

4.8.2 Oxidative Stress Activity (ROS Quantification)

The potential to eliminate Reactive Oxygen Species (ROS) is a key factor in the wound healing process. To evaluate the antioxidant activity of the produced membranes, a ROS quantification assay was performed. For this assay, HFFF2 were seeded in a 96-well plate at a density of 25,000 cells/cm² and incubated for 24 hours. The membrane extracts were sterilized by placing them in an oven at 120°C for 2 hours and then incubated for 1 hour in 20 % Tris buffer (pH = 7.5) in DMEM-LG. After the cells' incubation, they were treated with 50 µM hydrogen peroxide (H_2O_2) in PBS for 30 minutes, followed by treatment with the membrane extracts for an additional 24 hours. After this period, the cells were washed with PBS and treated with 10 µM 2',7'-dichlorofluorescein diacetate (DCFDA) (Sigma-Aldrich) in PBS for 30 minutes. The assay included several control groups: cells not treated with hydrogen peroxide, cells treated with hydrogen peroxide without extract, and cells pre-treated with ascorbic acid for 1 hour before the addition of DCFDA. The samples were normalized to the control treated with hydrogen peroxide, as positive control, and the results were expressed as *mean ± standard deviation*. The fluorescence was measured at excitation and emission wavelengths of 480 nm and 530 nm, respectively, using Biotek Synergy | LX .

4.8.3 Adhesion and Proliferation

To evaluate the viability and compatibility of the produced membranes with HFFF2, adhesion and proliferation assays were performed. The membranes were cut into 15 mm diameter discs and sterilized in an oven at 120 °C for two hours. For this assay, a 24-well plate was used, with each well containing a membrane secured with an O-ring on top, resulting in 1 cm² available area. After plate assembly, the membranes were left in medium for one day and washed twice before cell seeding. Controls included wells with the membranes and O-ring but only medium (material control) and wells with glass

coverslips and O-ring (cell control). The HFFF2 cell suspension was prepared according to the procedure in Appendix C.1, achieving a concentration of 15,000 cells/cm², which was then seeded into the wells. After assembly and seeding, the plate was incubated at 37 °C with 5 % CO_2. Cell viability on the scaffolds was assessed using a resazurin assay on days 1, 4, 7 and 11 post-seeding, as described in Appendix C.2. At least five replicates were used in each experiment and three biological replicates were performed to ensure reproducibility of the results. The samples were normalized to the cell control of the day 1, and the results were expressed as *mean ± combined standard uncertainty*.

4.8.3.1 Cell Morphology

To evaluate the morphology of cells adhered to the membranes during the proliferation assay, one replicate from each membrane group and a cell control were fixed for Phalloidin and DAPI staining analysis in day 7 of the three assay replicates. The fibers and coverslips containing cells were washed three times with PBS 1x, and fixation was carried out using 4 % paraformaldehyde (PFA) for 20 minutes. After fixation, the samples were washed three more times with PBS 1x to remove any residual fixative. Cell membranes were permeabilized using 0.3 % Triton X-100 (v/v in PBS) for 15 minutes, and the samples were washed again three times with PBS. Subsequently, the samples were incubated with phalloidin i-Fluor 555 conjugate (1:1000, Cayman) for 90 minutes at room temperature, protected from light, to stain the actin filaments. Following this step, the samples were washed three more times with 1x PBS. Nuclear staining was performed with 10 µM DAPI (4,6-diamidino-2-phenylindole, Molecular Probes) in PBS for 5 minutes, and the samples were washed with PBS followed by deionized water to remove salts. The samples were then mounted on slides using Mowiol mounting medium (Sigma-Aldrich). The slides were left to dry overnight at room temperature, protected from light, and subsequently stored at 4 °C until observation using a Nikon Eclipse Ti-S microscope.

4.9 Statistic Methods

The results are expressed as mean ± standard deviation or, for cell studies, as mean ± combined standard uncertainty. Statistical analysis of the cell studies was carried out using a one-way ANOVA followed by Tukey's post hoc test, with significance set at $^*p < 0.05$.

5

Results and Discussion

5.1 Characterization of Electrospun Membranes

5.1.1 Scanning Electron Microscopy (SEM)

The concentrations of both the polymer and any drugs added to the solution significantly influence the success of the membranes formation [41]. Therefore, SEM analysis was essential to understand how Quer and AgNPs might affect the membrane morphology and diameter. In Figure 5.1, SEM images of the membranes with different concentrations of Quer and those containing AgNPs are shown. All the membranes showed a regular shape without defects. Using *ImageJ* software, the average diameters of the fibers were determined to be (255 ± 55) nm, (310 ± 50) nm, (337 ± 56) nm, and (181 ± 37) nm for the 2 % CS + 2 % GEL membranes containing 1.25 % Quer, 2.5 % Quer, 5 % Quer, and 1:200 AgNPs, respectively. Additionally, the 2 % CS - 2 % GEL membrane had an average diameter of (263 ± 51) nm. Although the membranes compositions are different, Vashisth et al. (2015) concluded that an increase in Quer in poly(ε-caprolactone-co-lactide) (PCLA) and PCL membranes would cause a larger diameter [24]. Similarly, G.Ajmal found that Quer administration in PCL-GEL membranes increased their diameter [38]. Both studies support the results obtained in this study using CS and GEL membranes, where higher Quer content was associated with a tendency for larger fiber diameters. However, this increase was not statistically different based on the images analyzed.

On the other hand, membranes containing AgNPs have a much smaller diameter due to the increased conductivity of the initial solution for electrospinning. Consequently, during the electrospinning process, the fiber deposition is faster, resulting in membranes with small diameters [50].

Backscattered SEM images provide insight into the distribution of elements within the samples. Silver, being a heavy element, scatters incident electrons more efficiently than lighter elements such as carbon and oxygen, the main components of the polymers, resulting in a brighter appearance in SEM images.

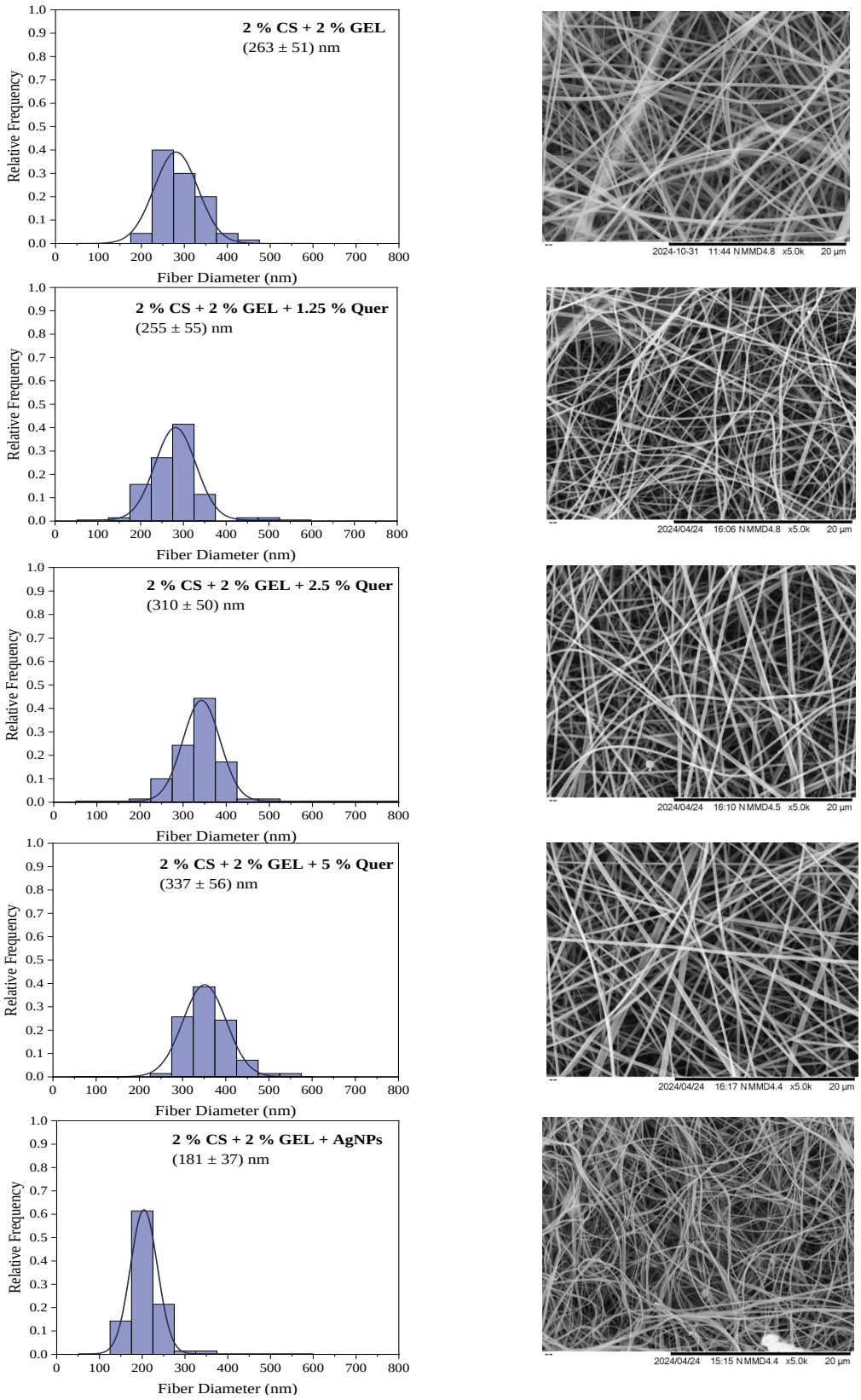

Figure 5.1: Diameter distribution graphs (left) and corresponding SEM images (right) of the polymeric standard CS-GEL membrane, membranes with 1.25 %, 2.5 %, and 5 % Quer, and the membrane containing AgNPs. The scale bar represents 20 µm.

Using ultra-high-resolution SEM in backscattered mode, it was possible to observe the successful incorporation of AgNPs within the CS-GEL + 1:200 AgNPs and CS-GEL + 2.5 % Quer + AgNPs membranes. The images of the membranes incorporated only with AgNPs and the EDS elemental analysis of components, including individual Ag, in the membranes CS-GEL + AgNPs and CS-GEL + Quer + AgNPs are shown in Appendix A, indicate the presence of Ag, which is most notable in the CS-GEL + AgNPs membrane. This may be due to a poorer incorporation of AgNPs into the membrane with Quer, or it could be that the Quer surrounding the nanoparticles makes their detection more difficult.

For membranes incorporated with Quer and AgNPs, membranes diameters were measured using the same method as previously described, based on high-resolution SEM images (Figure 5.2). The average fiber diameter was (223 ± 30) nm, which is an intermediate value between the diameters of membranes containing only AgNPs and those with 2.5 % Quer. White spots are also visible in these images, indicating the successful incorporation of nanoparticles into the membranes.

Notably, in Figure 5.3 a faint whitish cloud was observed surrounding the AgNPs. This might potentially be attributed to the hypothesis that quercetin interacts with and encapsulates the AgNPs, influencing their distribution within the membranes.

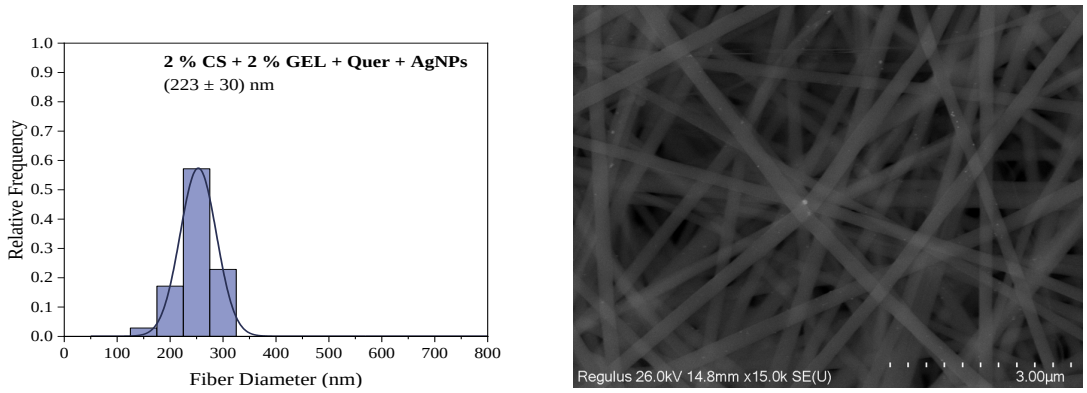

Figure 5.2: Diameter distribution graph (left) and corresponding SEM image (right) of the membrane containing 2.5 % Quer and AgNPs. The scale bar represents 3 µm.

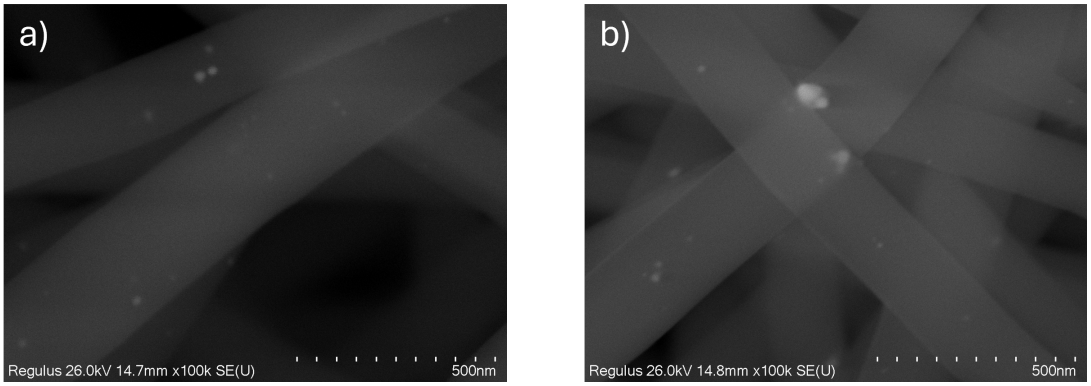

Figure 5.3: Ultra-high-resolution SEM images in backscattered mode for: a) CS-GEL + AgNPs membrane; b) CS-GEL + Quer + AgNPs membrane. The scale bar of the SEM images represents 500 nm.

5.1.2 Fourier Transform Infrared Spectroscopy (FTIR)

The FTIR spectra of the different membrane compositions were analyzed to determine the functional groups present and their interactions within the composite membrane. The analysis compared the spectra of pure GEL, CS, and Quer with those of the produced membranes. In Figure 5.4, the FTIR spectrum of GEL exhibited characteristic peaks indicating the presence of amide groups and other functional groups. Key peaks included: 3280 cm^{-1}, Amide A (N-H stretching); 1637 cm^{-1}, Amide I (C=O stretching); 1537 cm^{-1}, Amide II (N-H bending); 1440 cm^{-1}, CH_2 stretching; 1240 cm^{-1}, Amide III (C-N stretching); 2933 cm^{-1}, CH_2 bending. These peaks, present in the FTIR of pure GEL, were also found in the membranes, confirming the presence of peptide bonds from the GEL [51].

The FTIR spectrum of CS also showed characteristic peaks corresponding to its hydroxyl and amide groups, such as: 3300 cm^{-1}, O-H stretching; 1655 cm^{-1}, Amide I (C=O stretching); 1590 cm^{-1}, Amide II (N-H bending); 1249 cm^{-1}, Amide III; 1021 cm^{-1}, Saccharide groups (C-O stretching) [32, 52]. In the CS-GEL membrane, peaks from both GEL and CS were observed, some with slight shifts, possibly due to the interactions between the polymers. The addition of PEO or CA for crosslinking could also influence some of the bonds present. However, since the compositions of the two polymers used for the membranes are predominantly organic and amide groups, their characteristic peaks are very close in wavenumber, making it challenging to distinctly differentiate between the GEL and CS bonds in the membranes. The incorporation of CA into the membranes results in the formation of amide and imide bonds due to reactions between the carboxylic groups of CA and the amine groups of the polymers used, both GEL and CS. Notably, while some characteristic peaks of CA are not clearly visible, the peak at 1710 cm^{-1} stands out in the spectra of the crosslinked membranes. This peak is associated with the C=O stretching of carbonyl groups in the newly formed amide and imide bonds, confirming effective crosslinking [53]. The CS-GEL + AgNPs membrane did not show significant differences compared to the CS-GEL membrane, with some shifts possibly related to interactions between the AgNPs and the polymers.

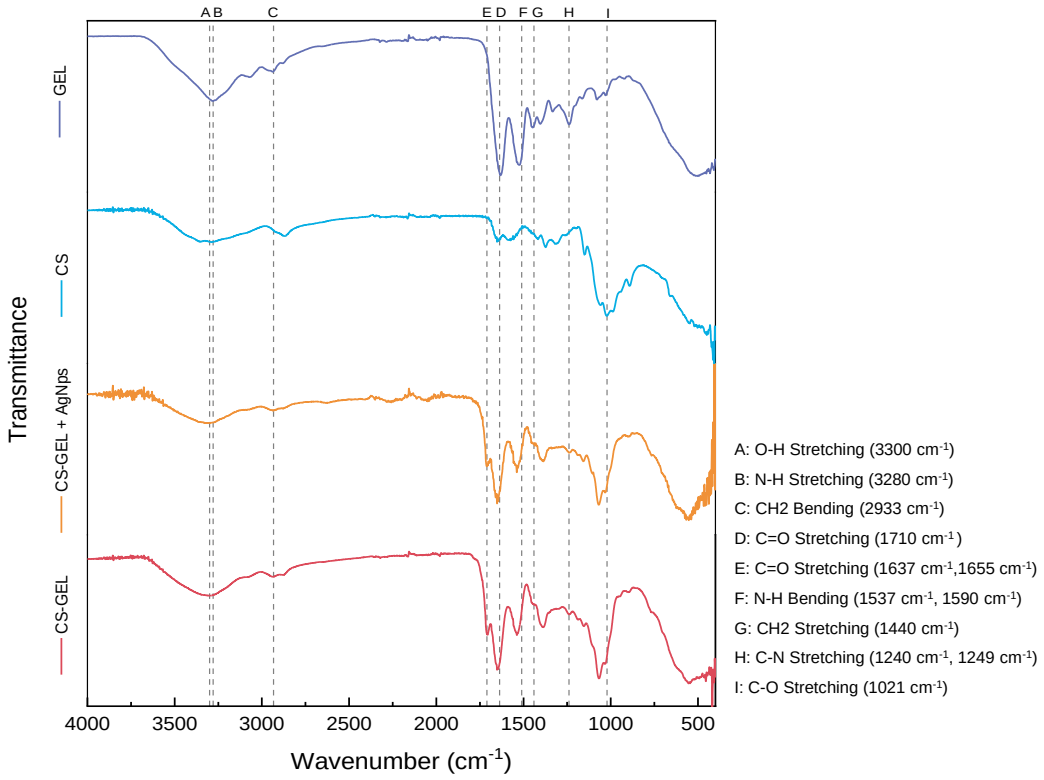

Figure 5.4: FTIR Spectra of GEL, CS, CS-GEL + AgNPs membrane and CS-GEL membrane.

Figure 5.5 presents the spectra of pure Quer, CS-GEL + Quer, CS-GEL + Quer + AgNPs and CS-GEL membranes. Pure Quer's spectra show typical peaks of aromatic rings at 1610 cm^{-1}, 1560 cm^{-1}, and 1510 cm^{-1}, corresponding to C=C aromatic ring stretch bands. The peak at 1664 cm^{-1} represents the aryl ketone C=O stretching, whereas the peak at 3300 cm^{-1} indicates the stretching of hydroxyl groups in Quer [38, 54].

In the spectra of CS-GEL membranes with Quer, the presence of Quer can be identified by the additional peaks corresponding to its characteristic functional groups. However, these peaks are very close to those found in the pure polymer spectra in Figure 5.4, making it challenging to distinctly differentiate the contributions of Quer, GEL, and CS. The slight shifts in peak positions in the composite membranes may be attributed to the interactions between the polymers and Quer, which could modify the bonding environment, resulting in the observed shifts.

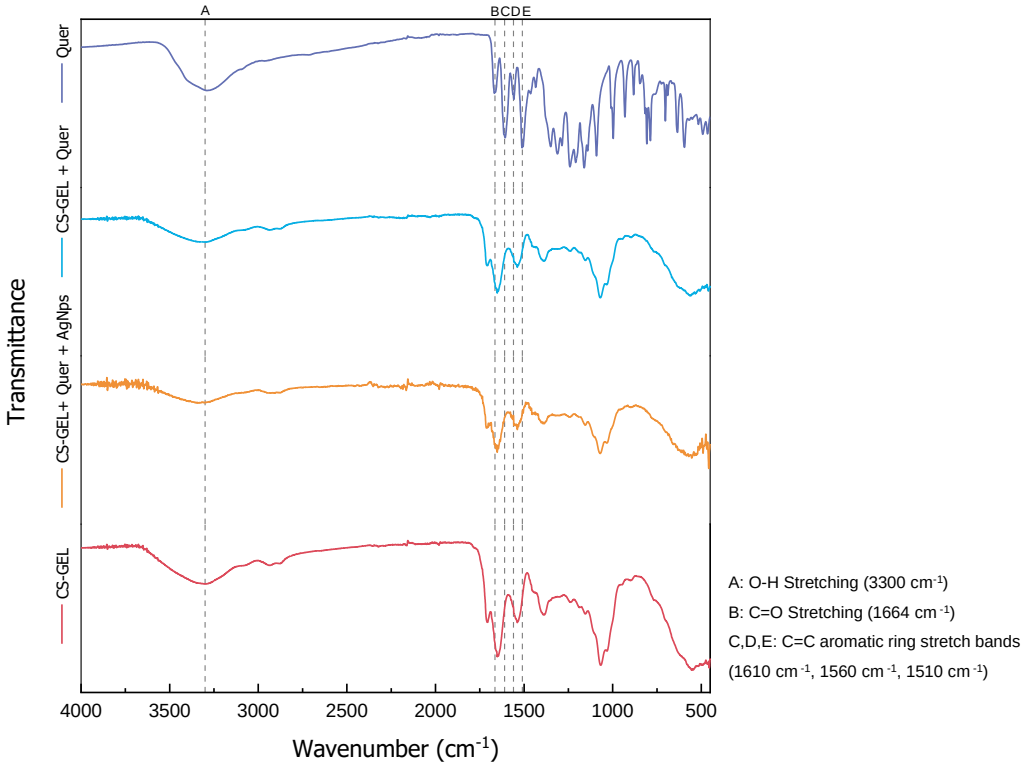

Figure 5.5: FTIR Spectra of Quer, CS-GEL + Quer membrane, CS-GEL + Quer + AgNPs membrane and CS-GEL membrane.

5.1.3 Characterization of AgNPs

The AgNPs solution produced using the chemical method described in 4.1 exhibited a yellow-brown color, which is generally indicative of successful nanoparticle synthesis. To initially confirm the presence of nanoparticles in the solution, 100 µL of the sample was diluted in 3 mL of water, resulting in a 0.95 mM solution. This dilution prevents saturation and maintains the absorbance values within the spectrophotometer detection limits. As expected, the resulting solution displayed a yellow hue. AgNPs typically exhibit absorption peaks within the range of 390-470 nm, depending on their size [55]. In Figure 5.6, a distinct peak around 390 nm can be observed, which confirms the presence of AgNPs in our solution. The evaluation of the AgNPs' diameter was performed using DLS. The diameter of the AgNPs was found to be (23.32 ± 1.43) nm, with aggregates measuring (70.93 ± 5.65) nm, contributing approximately equally to the overall particle distribution. To consider a solution of uniform nanoparticles, values of Polydispersity Index (PDI) have to be equal to or below 0.2, indicating that, despite the presence of aggregates, the overall size distribution remains moderately uniform [56, 57].

The size and shape of the particles can be influenced by the synthesis process, and similar studies using this method have reported particle diameters within a comparable range, further supporting the reliability of the results, such as the 25.92 nm diameter

reported by Kong et al. [58, 59].

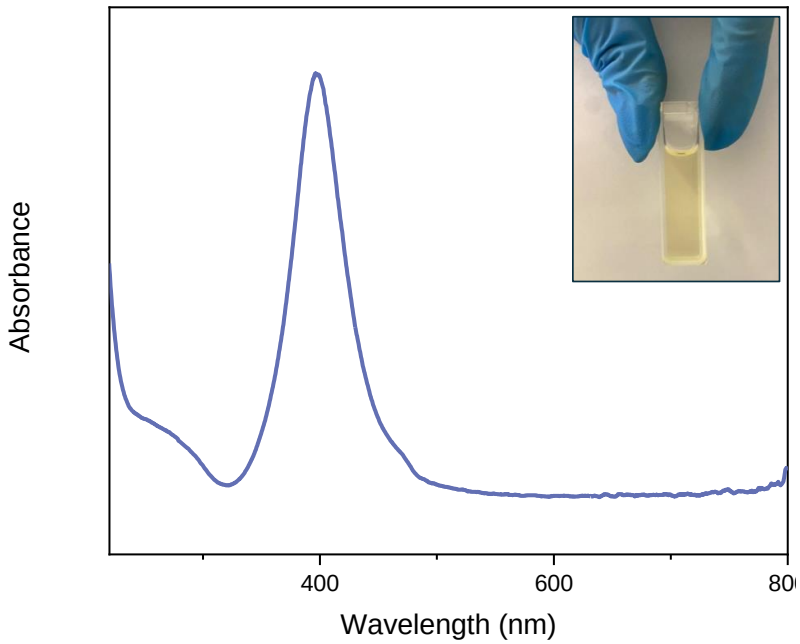

Figure 5.6: UV-Vis spectrum of the synthesized AgNPs in a concentration of 0.95 mM in water, with an inset image of the solution in a cuvette.

5.2 Release Assays

5.2.1 Quercetin Release Assay

Drug delivery is one of the most promising electrospinning applications because of its high loading capacity and encapsulation efficiency [60]. Given the variety of methods described in the literature, optimizing this protocol was a challenge in order to achieve the desired cumulative release curve from the membranes under study. Through these trials, it was successfully obtained curves with the desired profile using the protocol described in Section 4.6.1. The calibration curve of Quer, detailed in Appendix D, was essential to obtain the Quer release curves, allowing the conversion of absorbance data obtained from the spectrophotometer into the amount of quercetin released.

All the Quer release curves, whether from membranes with different concentrations or under different pH conditions, exhibited similar profiles. An initial burst release was observed, particularly within the first hour, followed by a slower release over the course of 48 hours. In Figure 5.7, the release profile and cumulative mass of Quer over the 24-hour testing period can be seen. This release profile is particularly beneficial for chronic wounds, as the initial burst provides immediate protection during the early inflammatory phase following tissue injury, while the subsequent sustained release ensures prolonged delivery of the drug [60].

As the concentration of Quer in the membranes increased, so did the cumulative mass released. For membranes containing 1.25 % Quer, the maximum amount released after 48

hours was 52 µg, 64 µg, and 73 µg in buffers with pH 5.6, pH 7.4, and pH 8, respectively. The release profile of these membranes was more controlled over time, although the cumulative mass released was relatively low compared to other membranes. For the CS-GEL + 2.5 % Quer membranes, the maximum release after 24 hours was 73 µg, 79 µg, and 94 µg in pH 5.6, pH 7.4, and pH 8 buffers, respectively. These profiles showed a more pronounced initial release followed by a more controlled release, which is desirable for ensuring a beneficial amount of drug release while maintaining controlled delivery. In membranes with the highest concentration of Quer the cumulative mass released after 24 hours exceeded 120 µg in all conditions, with a very rapid release profile within the first hour, indicating less controlled release. This initial rapid release is likely due to Quer present on the surface of the membrane dissolving within the first few hours, resulting in the observed burst release. The subsequent controlled release of the remaining Quer can be attributed to its gradual diffusion through the membrane as it remains immersed in the solution [41, 61]. C. Ulker Turan and Y. Guvenilir stated in their study that drug release from membranes composed of hydrophilic polymers, such as GEL and CS, tends to be faster. The strong crosslinking provided by CA gives the matrix a stable structure, making it ideal for sustaining a controlled release of the drug [62].

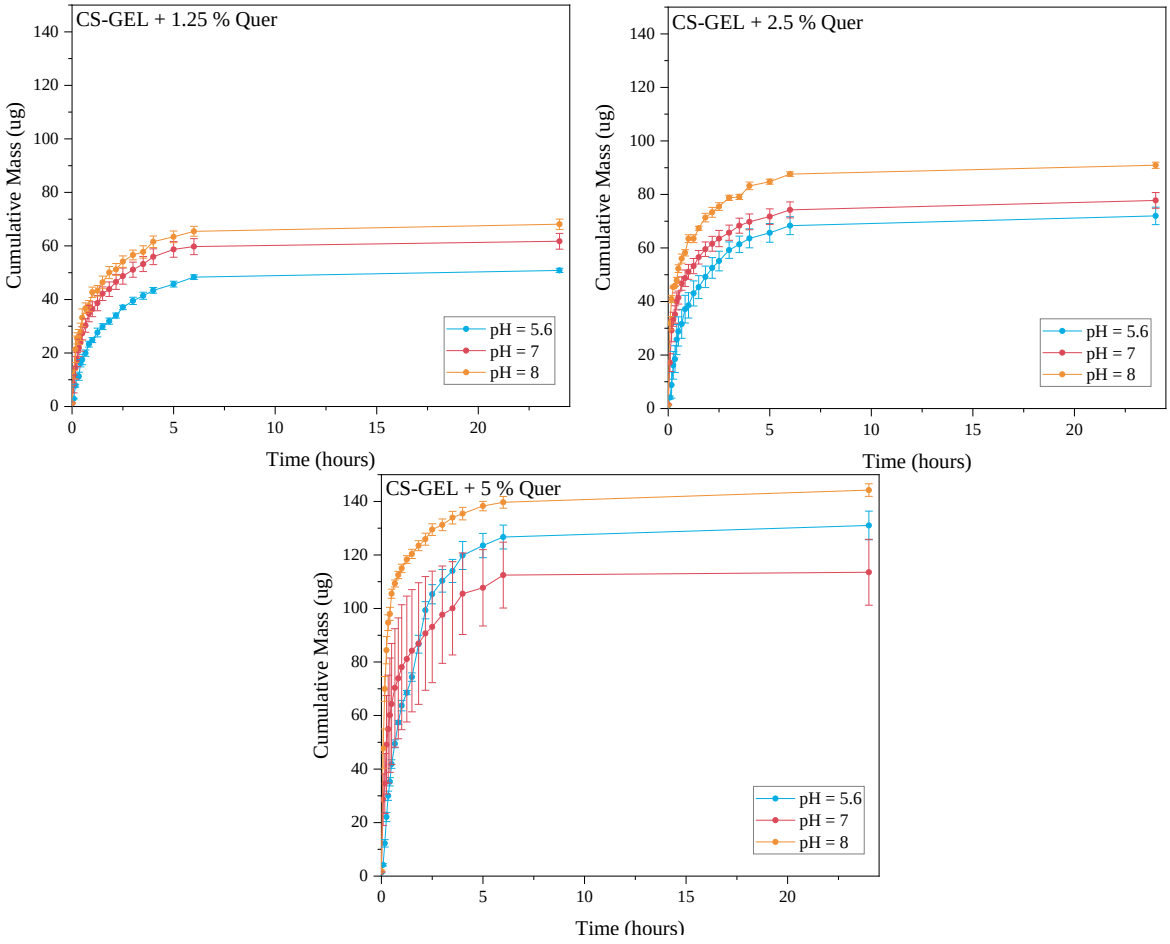

Figure 5.7: Cumulative Quer release profiles over 24 hours at different pH values (5.6, 7.0, and 8.0) for CS-GEL membranes containing 1.25 %, 2.5 %, and 5 % (w/w) of Quer.

Based on this evaluation and considering the cytotoxicity values of Quer (refer to Section 5.3.1), a concentration of 2.5 % (w/w) Quer was selected for further experiments, including the preparation of CS-GEL + Quer + AgNPs membranes. The graphs also indicate that the more basic solution, which mimics skin wound conditions with pH 8, resulted in a higher cumulative mass release. This outcome aligns with expectations, as the goal is to achieve a controlled release with sufficient concentration to enhance wound healing. This could be attributed to the stronger crosslinking effect of CA in acidic environments, which increases the rigidity of the membrane, thereby making more difficult the diffusion and subsequent release of Quer [60].

5.2.2 Inductively Coupled Plasma (ICP)

ICP analysis was conducted to evaluate the silver ion release from membranes containing AgNPs. Measurements were taken at two time points: 6 and 24 hours, with the membranes immersed in PBS with 0.02 % Tween 80 to simulate one of the conditions used in the Quer drug release assay. For both types of membranes tested, the concentrations of silver ions released were consistent across the two time points. Although the release represented only a small percentage of the theoretical amount added into the electrospinning solution, it is hypothesized that the majority of the release occurs within the first 6 hours, stabilizing thereafter. This pattern resembles the release profile observed and discussed in the Quer release study.

Table 5.1: Results for silver ion release from CS-GEL + AgNPs and CS-GEL + Quer + AgNPs membranes at 6 h and 24 h after release in PBS. The results are presented as Mean ± Standard Deviation (mg/L).

	CS-GEL + AgNPs	**CS-GEL + Quer + AgNPs**
6 h	0.368 ± 0.022	0.197 ± 0.046
24 h	0.369 ± 0.022	0.196 ± 0.046

The low concentration of nanoparticles in the polymeric solution, combined with their small diameter, supports the hypothesis of rapid release. Release kinetics of silver ions are influenced by particle size and the initial concentration of AgNPs. Smaller nanoparticles, with higher surface area and solubility, release ions more quickly than larger ones, consistent with thermodynamic principles [63].

The theoretical amount of silver in the membranes, based on the composition and concentration of the AgNPs, is 15.15 µg in 8 mL of the solution, corresponding to 1.89 mg/L. Significant differences in silver ion concentrations were observed between the CS-GEL + AgNPs membranes and the CS-GEL + Quer + AgNPs membranes. As shown in Table 5.1, membranes containing only AgNPs released up to 0.369 mg/L silver ions, whereas membranes incorporating also Quer released only 0.197 mg/L silver ions. This lower silver ions release in membranes with AgNPs and Quer may be related to the backscattered SEM observations in section 5.1.1(Figure 5.3) where a whitish cloud surrounding the AgNPs

was hypothesized to be Quer. This interaction may influence the release of silver ions by partially encapsulating nanoparticles.

5.2.3 DPPH Radical Scavenging Assay

To evaluate the antioxidant effects of the CS-GEL, CS-GEL + Quer, CS-GEL + AgNPs, and CS-GEL + Quer + AgNPs membranes, a DPPH assay was performed and the results are exposed in Figure 5.8, along with a table containing the statistical test results. Given the well-known high antioxidant activity of pure Quer, its activity was also measured at a concentration identical to that used in the electrospinning solution for membrane production.

The lower activity of the membranes compared to that of pure Quer, (93.66 ± 0.95) %, is likely due to several factors. First, Quer in its pure form reacts more readily with DPPH, whereas in the membrane, its release may be incomplete due to encapsulation. Additionally, the Quer might lose some of its antioxidant activity during the electrospinning process or between production and the assay due to partial oxidation [40].

The membranes containing only AgNPs showed no significant antioxidant activity, similar to the CS-GEL membrane. This confirms that AgNPs do not contribute to antioxidant activity under these conditions [64].

The CS-GEL + Quer membrane showed an antioxidant activity of (53.27 ± 3.31) %, which was statistically significantly different ($p < 0.05$) from all other membranes and pure Quer, except for the CS-GEL + Quer + AgNPs membrane (44.04 ± 8.67) %. Although the CS-GEL + Quer + AgNPs membrane showed a tendency toward lower antioxidant activity compared to the CS-GEL + Quer membrane, this difference was not statistically significant, considering the triplicates performed and the spread of results, which were close to those obtained for the membrane containing only Quer. These membranes demonstrated the highest antioxidant activity among the tested membranes derivated of the presence of Quer [22, 65]. This small variation in antioxidant activity could be related to interactions between Quer and AgNPs, as previously discussed in other sections, potentially affecting the release profile or reactivity of Quer. However, it can be concluded that the addition of AgNPs does not negatively impact the antioxidant activity of Quer within the membranes.

The antioxidant activity values observed for the CS-GEL + Quer and CS-GEL + Quer + AgNPs membranes fall within the medium range of DPPH inhibition. In this range, materials exhibit antioxidant properties that are considered moderate but still relevant for applications in wound dressing materials. These properties further highlight the potential of these membranes as bioactive components in wound care [66].

These two membranes were also subjected to the DPPH assay over time in PBS at 1, 3, and 6 hours to compare their behavior over the release period. As shown in Table 5.2, no significant differences were observed between the two membranes. However, a trend of increasing antioxidant activity over the time points was noted, which is likely associated with the gradual release of Quer from the membranes into the buffer.

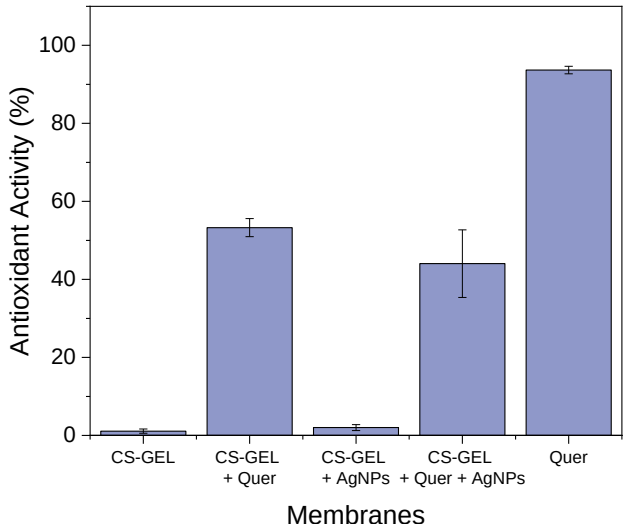

	Significance
Quer ; CS-GEL	*
Quer ; CS-GEL + AgNPs	*
Quer ; CS-GEL + Quer + AgNPs	*
CS-GEL + Quer ; CS-GEL	*
CS-GEL + Quer + AgNPs ; CS-GEL	*
Quer ; CS-GEL + Quer	*
CS-GEL + AgNPs ; CS-GEL + Quer	*
CS-GEL + Quer + AgNPs ; CS-GEL + AgNPs	*
CS-GEL + Quer + AgNPs ; CS-GEL + Quer	No significance
CS-GEL + AgNPs ; CS-GEL	No significance

Figure 5.8: Antioxidant activity (%) of CS-GEL, CS-GEL + Quer, CS-GEL + AgNPs, and CS-GEL + Quer + AgNPs membranes measured using the DPPH assay. The right panel presents the statistical significance (*p < 0.05) of pairwise comparisons between the membranes.

Table 5.2: Antioxidant activity results for CS-GEL + Quer and CS-GEL + Quer + AgNPs membranes at 1, 3, and 6 hours after release in PBS, measured using the DPPH assay. The results are presented as Mean ± Standard Deviation (%).

	CS-GEL + Quer	**CS-GEL + Quer + AgNPs**
1 h	38 ± 1.7	37 ± 5
3 h	39 ± 10	42 ± 1.2
6 h	42 ± 5	46 ± 5

5.3 *In Vitro* Tests

5.3.1 Cytotoxicity Assays

ISO 10993-5 classifies results as non-toxic (above 80 %), gently toxic (60-80 %), highly toxic (40-60 %), or severely toxic (less than 40 %) [67]. ISO 10993-5 describes test methods to assess the *in vitro* cytotoxicity of medical devices, which involve the incubation of cultured cells in contact with extracts of a device, either directly or through diffusion. The cytotoxicity of the membranes was evaluated in accordance with the ISO 10993-5 standard [68].

The cytotoxicity assay with pure Quer was conducted on different cell lines: ??, HFFF2, and HaCat. This was performed to study the varying sensitivities of skin-related cells to the drug used in the membranes—Quer. In Figure 5.9, the graphs depict the cytotoxicity observed after 48 hours of exposing the cells to Quer, starting from a concentration of 500 µM, followed by a series of 1:2 dilutions.

The different cell lines exhibited varying reactions to pure Quer. HFFF2 showed slight toxic effects at concentrations of 500 µM and 250 µM, with viability around 80 % at 125 µM.

At concentrations of 62.5 µM and lower, the HFFF2 exhibited viability above 90 % with no significant cytotoxic effects.

HaCat cells were the least sensitive to Quer, showing only mild cytotoxic effects at 500 µM. From 250 µM and lower concentrations, these cells displayed no negative effects, with viability levels above 80 %.

The ?? cells were the most sensitive to Quer, with minimal or no cytotoxic effects only observed at concentrations bellow 15.63 µM. Higher concentrations resulted in viability values below 60 %, indicating moderate to severe toxicity.

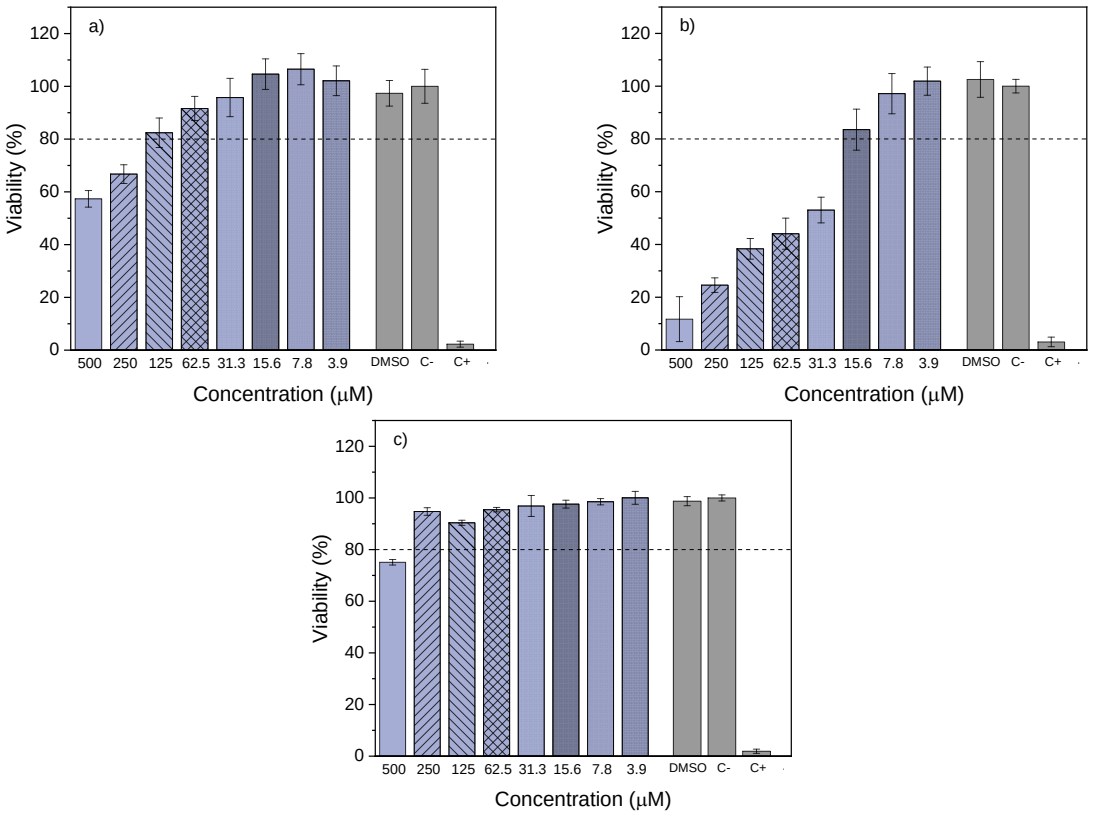

Figure 5.9: Cytotoxicity assessment of quercetin on different cell lines after 48 hours of incubation. The panels show the cell viability (%) for a) HFFF2, b) SH-SY5Y, and c) HaCat cell lines, exposed to Quer in sequential 1:2 dilutions, ranging from 500 µM to 3.9 µM. The dashed line at 80 % viability indicates the threshold below which Quer begins to exhibit cytotoxic effects. Data represent the mean ± standard deviation from three biological replicates, normalized to the negative control (C-). The positive control (C+) and DMSO control are also shown for comparison.

To analyze the cytotoxicity of the membranes containing AgNPs and Quer, assays were conducted using ?? cells and HFFF2, starting with a concentration of 15 mg/mL. This corresponds to approximately 0.375 mg of Quer and 74.6 µg of AgNPs per 15 mg of membranes. However, due to encapsulation efficiency previously discussed for quercetin in this work, it is expected that the actual released amounts are lower. ?? cells demonstrated higher sensitivity to increased membrane extract concentrations, as expected due to their neural origin. CS-GEL membranes did not exhibit cytotoxicity at the initial concentration, reflecting their inherent biocompatibility [60]. ?? cell viability above 80 % was observed

at extract concentrations equal to or below 3.25 mg/mL for CS-GEL + Quer membranes, which is comparable to the results obtained with CS-GEL + AgNPs membranes. This aligns with findings reported in the literature, where, for instance, Vero cells exhibited dose-dependent effects on cell viability with AgNPs, maintaining viability only at 4 mg/mL in PVP membranes containing a 1:200 ratio of AgNPs [44]. In the previous results of this work, we also observed that the concentration of Quer influences the viability of certain cell lines, such as ?? and HFFF2 (refer to pure Quer data in Figure 5.9).

The CS-GEL + 2.5 % Quer + AgNPs membranes demonstrated low toxicity in HFFF2 cell lines, even at higher extract concentrations. For ?? cells, they are considered non-toxic at concentrations above 7.5 mg/mL, which is higher compared to the CS-GEL + Quer and CS-GEL + AgNPs membranes. This difference may be attributed to the hypothesis that the combination of Quer and AgNPs alters the release profile of both Quer and silver ions, resulting in a more controlled release. Such controlled release likely reduces the immediate exposure of cells to potentially harmful concentrations, thereby enhancing cell viability.

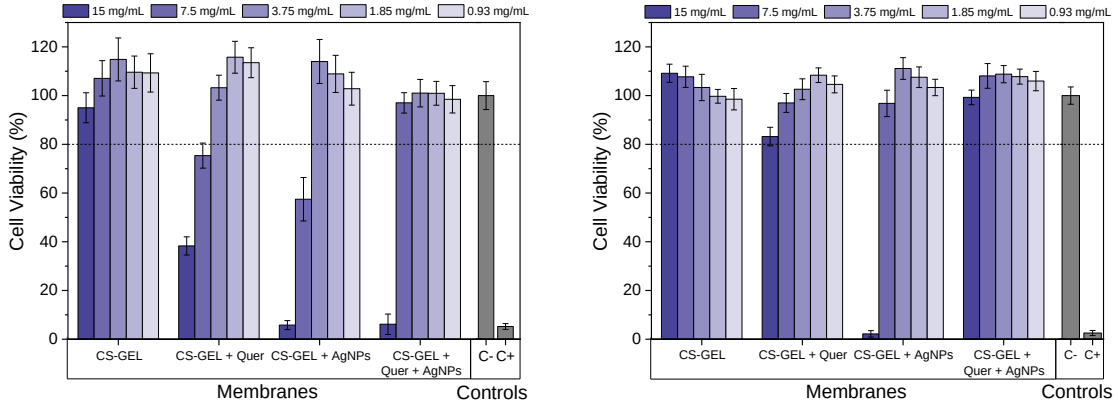

Figure 5.10: Cytotoxicity assessment of membranes containing quercetin and silver nanoparticles. Cell viability (%) of SH-SY5Y cells (left) and HFFF2 cells (right) after 48 hours of exposure to different concentrations (3.75, 7.5, 15, and 30 mg/mL) of extract of the membranes: CS-GEL, CS-GEL + Quer, CS-GEL + AgNPs, and CS-GEL + Quer + AgNPs. The dashed line at 80 % indicates the threshold for cytotoxic effects. Data represent mean ± standard deviation from three biological replicates, normalized to the negative control (C-). Positive controls (C+) are also shown for reference.

5.3.2 Reactive Oxygen Species (ROS)

ROS are essential during the initial inflammatory phase of wound healing, supporting the body's defense system through phagocytic activity. However, in wound environments such as severe trauma, excessive ROS generation can disrupt the healing process by causing oxidative damage to fibroblasts. Oxidative stress was evaluated using the DCFDA assay for all membranes at three different concentrations, including pure Quer and AgNPs, starting with concentrations approximating those found in the membranes. DCFDA is a non-fluorescent compound that, upon oxidation by ROS, becomes fluorescent and can

be measured spectrophotometrically [69]. The results of the ROS measurements under these conditions are shown in Figure 5.11. The data in these graphs were normalized to the positive control, which corresponds to the group exposed to H_2O_2, a treatment that induces elevated ROS levels and increases fluorescence. A control with ascorbic acid was also used to compare with the samples due to its strong antioxidant activity. Based on the analysis of the graphs, no statistically significant differences were observed between the various groups. However, the membrane containing AgNPs at a concentration of 15 mg/mL exhibited notably lower ROS measurement levels, likely due to cytotoxic effects at this concentration for HFFF2. This suggests that the reduced ROS levels may result from the lack of viable cells in the well. Although less pronounced, the 15 mg/mL concentration of the CS-GEL + Quer+ AgNPs membrane also demonstrated one of the lowest fluorescence values, indicating reduced ROS levels in the assay. It is well-known that Quer, as an antioxidant agent, has the ability to neutralize reactive oxygen species. Consequently, lower fluorescence values would be expected for pure Quer and membranes containing Quer [65, 70].

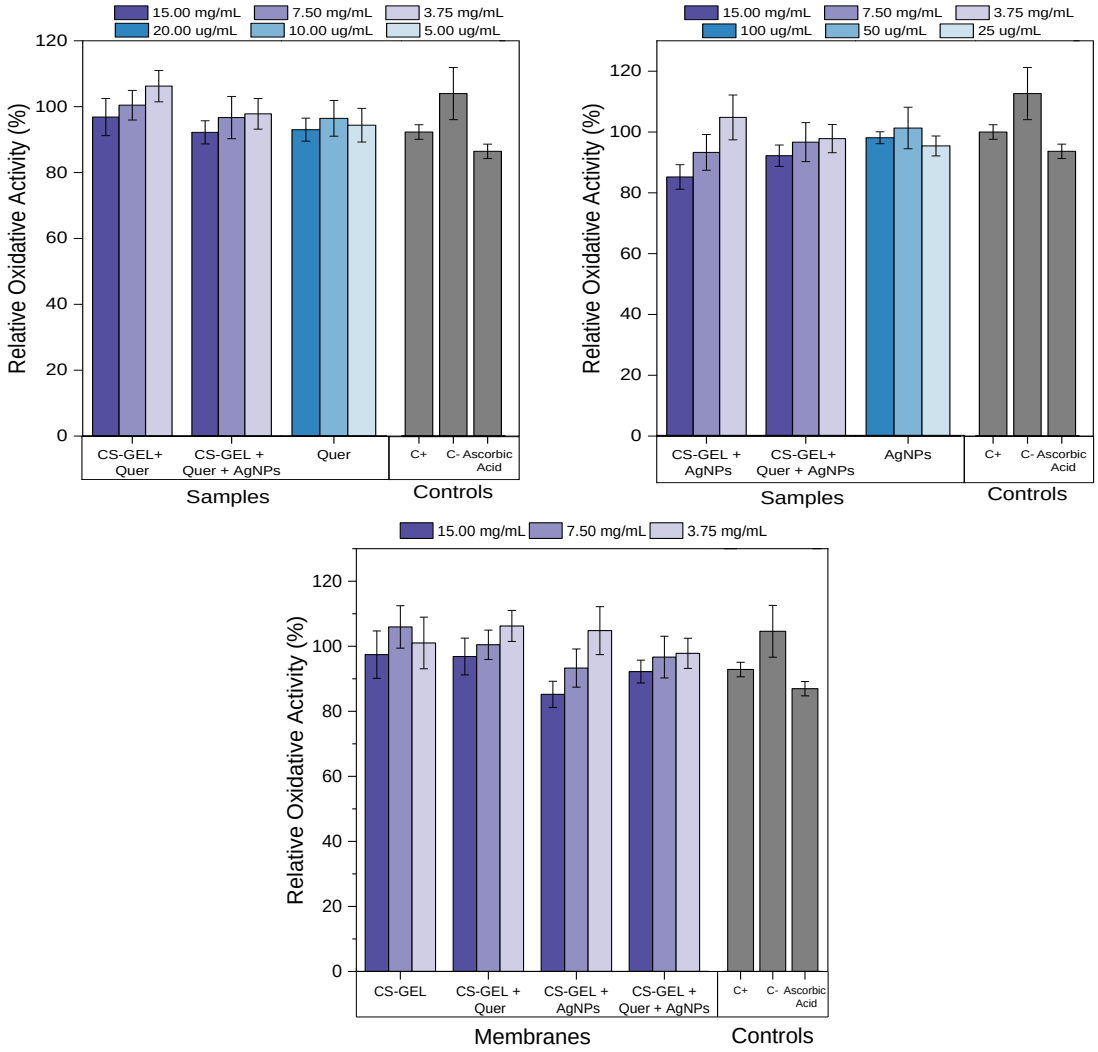

Figure 5.11: Oxidative stress reduction analysis of different membranes performing ROS Assay. Relative oxidative activity (%) of HFFF2 cells under different conditions. The top left panel shows the conditions containing Quer, the top right panel presents the conditions involving AgNPs, and the bottom panel illustrates the set of all four membranes: CS-GEL, CS-GEL + Quer, CS-GEL + AgNPs, and CS-GEL + Quer + AgNPs. Values were normalized to the positive control and are presented as mean ± standard deviation.

5.3.3 Adhesion and Proliferation

To evaluate the membranes' potential to support cell adhesion and proliferation, an assay was conducted over 11 days using three biological replicates. The first evaluation was performed 24 hours after cell seeding using a resazurin assay to determine cell adhesion, with subsequent measurements on days 4, 7, and 11 to evaluate cell proliferation. By referencing the initial viability data, along with material and resazurin controls, cell adhesion and proliferation were calculated over the 11-day period. On the first day, the membranes showed comparable adhesion values for HFFF2. Overall, as shown in Figure 5.12, a general trend of increased cell viability was observed across all membranes.

To better assess the proliferation potential of the membranes, the ratio between cell viability on day 11 and day 1 was calculated. Among the tested membranes, the CS-GEL

+ Quer membrane exhibited the highest ratio of 2.31, followed closely by the CS-GEL membrane, 2.19, with only a small difference between the two. The CS-GEL + Quer + AgNPs membrane followed with a ratio of 1.73, while the CS-GEL + AgNPs membrane showed the lowest ratio of 1.29.

The scaffold containing AgNPs showed the least improvement in cell population over the course of the assay. The lower proliferation observed in the AgNPs membrane can be attributed to the fact that AgNPs are known to cause dose-dependent adverse biological effects, including cytotoxicity and genotoxicity, as reported in several studies. Lower concentrations of AgNPs have been suggested to improve cell survival and proliferation [50].

CS-GEL membranes demonstrated strong cell proliferation throughout the experiment, consistent with the natural polymers' ability to support cell adhesion, which justifies their high cell viability compared to the other conditions. The membrane containing Quer showed a notable increase in cell viability, with values more than doubling from day 1 to day 11. This result aligns with previous studies highlighting Quer as a protective component that promotes fibroblast proliferation [38]. While not achieving the levels observed with the CS-GEL or CS-GEL + Quer, the membrane containing both Quer and AgNPs exhibited a significant increase in cell population over time, outperforming the silver-only membrane by the end of the assay.

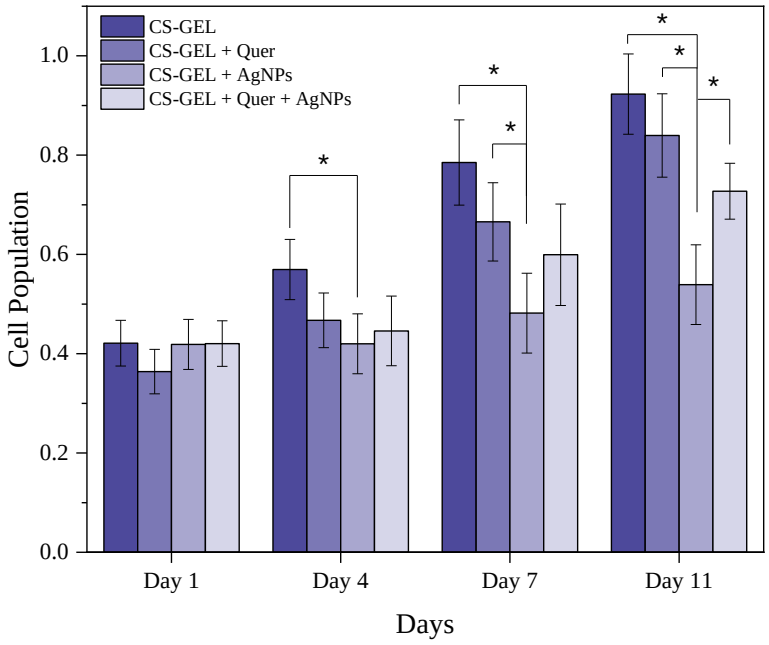

Figure 5.12: Relative Cell Population and proliferation of HFFF2 on different membranes. Results for CS-GEL, CS-GEL + Quer, CS-GEL + AgNPs, and CS-GEL + Quer + AgNPs membranes over 11 days of incubation. Adhesion is expressed as a normalized value relative to Day 1. Data are presented as mean ± standard deviation from three biological replicates. Statistical significance (*p < 0.05) is indicated for comparisons between membranes.

5.3.3.1 Cells Morphology

To evaluate the morphology of the cells on day 7 of the proliferation assay under different membrane conditions, DAPI and Phalloidin stainning was performed, to visualize the cell nuclei in blue and cytoskeleton in red, respectively. The images for each membrane and the control are shown in Figure 5.13. The CS-GEL membrane and the CS-GEL + Quer membrane were among the easiest to visualize, showing cells with long actin filaments. A high number of cells growing in clusters was observed in these membranes compared to others. This observation aligns with the adhesion and proliferation assay results, which showed that, on day 7, the CS-GEL membrane and the CS-GEL + Quer membrane exhibited the highest viability ratios. The tendency of cells to form clusters on these membranes, particularly the type observed in Figure 5.13 b), could be attributed to the non-uniform distribution of charges of CS, as hypothesized in previous studies [31].

Fibroblast shape is determined by focal adhesions that connect transmembrane proteins to the actin cytoskeleton [71]. Although cells were also visible on the CS-GEL + AgNPs membrane and the CS-GEL + Quer + AgNPs membrane, their density was noticeably lower at the same magnification compared to the previously mentioned membranes, this might be due to the fact that AgNPs could influence these focal points that HFFF2 need to form or due to some long-term cytotoxic effect caused by AgNPs. Between these two, the CS-GEL + Quer + AgNPs membrane exhibited slightly higher adhesion and proliferation in the quantitative assay.

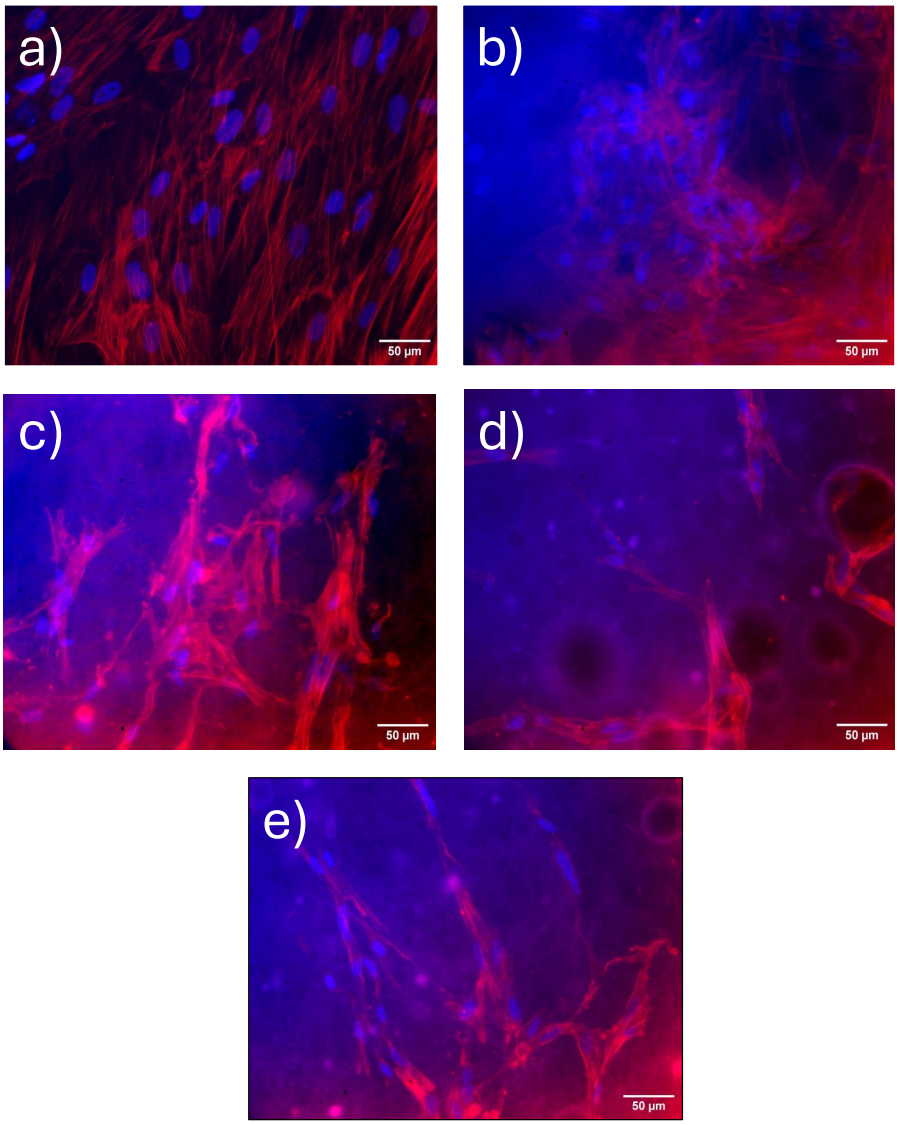

Figure 5.13: Fluorescent staining of cells cultured on different membranes after 7 days usign DAPI and Phalloidin. a) Control group: fibroblasts seeded directly on the plate; b) CS-GEL membrane; c) CS-GEL + Quer membrane; d) CS-GEL + AgNPs membrane; e) CS-GEL + Quer + AgNPs membrane. Nuclei were stained with DAPI (blue), and the cytoskeleton was stained with Phalloidin (red). Scale bar: 50 μm.

6

Conclusion and Future Work

This study demonstrated the potential of multifunctional electrospun membranes composed of GEL, CS, Quer, and AgNPs for enhanced wound healing applications. The combination of these components provided a robust framework for addressing key challenges in chronic wound treatment, including persistent inflammation, oxidative stress, and microbial infections.

Although there are existing studies on Quer and AgNPs separately, the innovation here lies in combining both components within a single membrane made from natural polymers. The incorporation of Quer provided antioxidant properties, while AgNPs imparted antimicrobial effects. Systematic characterization and *in vitro* assays demonstrated the membranes ability to support fibroblast adhesion and proliferation, with optimized drug release profiles and promising structural integrity.

The findings support the hypothesis that the interaction between Quer and AgNPs influences their respective release profiles, leading to a more controlled and synergistic release. This interaction not only enhances the membranes' antimicrobial and antioxidant properties but also improves their biocompatibility by reducing cytotoxicity at higher concentrations, while maintaining effective antioxidant activity. This controlled release mechanism presents an exciting avenue for future exploration, as it suggests that the combination of these components offers a dual benefit: bioactivity and cellular viability at more tolerable concentrations.

Future work should focus on further characterizing the antimicrobial potential of the AgNPs incorporated within the membranes, particularly under biologically relevant conditions. Evaluating silver ion release in environments containing proteins, such as FBS, could provide valuable insights into how biomolecular interactions influence release dynamics.

Further studies on ROS modulation remain critical, given Quer's potential to mitigate oxidative stress during wound healing. Clarifying whether the current outcomes are influenced by low concentrations or complex interactions between Quer and AgNPs would significantly deepen our understanding of these systems.

To continue the evaluation and study of the obtained membranes, enzymatic and

hydrolytic degradation assays, swelling tests, and mechanical tests should be conducted to complete the characterization. Additionally, the crystalline struture of AgNPs should be assessed using X-ray diffraction (XRD).

Beyond specific assays, advancing this work requires optimizing parameters for membranes production to improve reproducibility in cell adhesion and proliferation results. Continued efforts in this direction will ensure the scalability and robustness of the membranes for broader *in vitro* studies. Ultimately, validating these membranes *in vivo* wound models is a necessary step to establish their clinical relevance and effectiveness. By addressing these challenges and refining the system, the membranes developed in this study hold significant promise for advancing regenerative medicine. They represent a novel approach to chronic wound management, combining antimicrobial, antioxidant, and regenerative properties to improve clinical outcomes and enhance patients' quality of life.

Bibliography

[1] J. M. Lourenço. *The NOVAthesis LaTeX Template User's Manual*. NOVA University Lisbon. 2021. URL: https://github.com/joaomlourenco/novathesis/raw/main/template.pdf (cit. on p. i).

[2] J. R. Yu et al. "Current and Future Perspectives on Skin Tissue Engineering: Key Features of Biomedical Research, Translational Assessment, and Clinical Application". In: *Advanced Healthcare Materials* 8.5 (2019-03). ISSN: 21922659. DOI: 10.1002/adhm.201801471 (cit. on pp. 1, 9).

[3] C. Huang et al. "Anti-inflammatory hydrogel dressings and skin wound healing". In: *Clinical and Translational Medicine* 12.11 (2022-11). ISSN: 2001-1326. DOI: 10.1002/ctm2.1094 (cit. on p. 1).

[4] A. Amirsadeghi et al. "Vascularization strategies for skin tissue engineering". In: *Biomaterials Science* 8.15 (2020-08), pp. 4052–4073. ISSN: 20474849. DOI: 10.1039/d0bm00266f (cit. on p. 2).

[5] P. Kolimi et al. "Innovative Treatment Strategies to Accelerate Wound Healing: Trajectory and Recent Advancements". In: *Cells* 11.15 (2022-08). ISSN: 20734409. DOI: 10.3390/cells11152439 (cit. on p. 2).

[6] F. Urciuolo et al. "Bioengineered skin substitutes: The role of extracellular matrix and vascularization in the healing of deep wounds". In: *Journal of Clinical Medicine* 8.12 (2019-12). ISSN: 20770383. DOI: 10.3390/jcm8122083 (cit. on p. 2).

[7] M. Norouzi et al. "Advances in Skin Regeneration: Application of Electrospun Scaffolds". In: *Advanced Healthcare Materials* 4.8 (2015-06), pp. 1114–1133. ISSN: 21922659. DOI: 10.1002/adhm.201500001 (cit. on pp. 3, 4).

[8] A. D. Juncos Bombin, N. J. Dunne, and H. O. McCarthy. "Electrospinning of natural polymers for the production of nanofibres for wound healing applications". In: *Materials Science and Engineering C* 114 (2020-09). ISSN: 18730191. DOI: 10.1016/j.msec.2020.110994 (cit. on pp. 3, 4).

[9] C. Henriques et al. "A systematic study of solution and processing parameters on nanofiber morphology using a new electrospinning apparatus". In: *Journal of Nanoscience and Nanotechnology*. Vol. 9. 6. 2009-06, pp. 3535–3545. DOI: 10.1166/jnn.2009.NS27 (cit. on p. 3).

[10] A. Rogina. "Electrospinning process: Versatile preparation method for biodegradable and natural polymers and biocomposite systems applied in tissue engineering and drug delivery". In: *Applied Surface Science* 296 (2014-03), pp. 221–230. ISSN: 01694332. DOI: 10.1016/j.apsusc.2014.01.098 (cit. on p. 3).

[11] C. Cui et al. "Electrospun chitosan nanofibers for wound healing application". In: *Engineered Regeneration* 2 (2021-01), pp. 82–90. ISSN: 26661381. DOI: 10.1016/j.engreg.2021.08.001 (cit. on p. 5).

[12] M. E. Hoque et al. "Electrospun Matrices from Natural Polymers for Skin Regeneration". In: *Nanostructured Polymer Composites for Biomedical Applications*. Elsevier, 2019-01, pp. 87–104. ISBN: 9780128167717. DOI: 10.1016/B978-0-12-816771-7.00005-3 (cit. on p. 5).

[13] S. Ranganathan, K. Balagangadharan, and N. Selvamurugan. "Chitosan and gelatin-based electrospun fibers for bone tissue engineering". In: *International Journal of Biological Macromolecules* 133 (2019-07), pp. 354–364. ISSN: 18790003. DOI: 10.1016/j.ijbiomac.2019.04.115 (cit. on pp. 5, 6).

[14] N. Shafagh, M. Sabzi, and M. J. Afshari. "Development of pH-sensitive and antibacterial gelatin/citric acid/Ag nanocomposite hydrogels with potential for biomedical applications". In: *Journal of Polymer Research* 25.12 (2018-12). ISSN: 15728935. DOI: 10.1007/s10965-018-1661-9 (cit. on pp. 5, 6).

[15] I. Lukin et al. "Progress in Gelatin as Biomaterial for Tissue Engineering". In: *Pharmaceutics* 14.6 (2022-06). ISSN: 19994923. DOI: 10.3390/pharmaceutics14061177 (cit. on p. 5).

[16] S. R. Gomes et al. "In vitro evaluation of crosslinked electrospun fish gelatin scaffolds". In: *Materials Science and Engineering C* 33.3 (2013-04), pp. 1219–1227. ISSN: 09284931. DOI: 10.1016/j.msec.2012.12.014 (cit. on p. 6).

[17] K. Jalaja et al. "Potential of electrospun core-shell structured gelatin-chitosan nanofibers for biomedical applications". In: *Carbohydrate Polymers* 136 (2016-01), pp. 1098–1107. ISSN: 01448617. DOI: 10.1016/j.carbpol.2015.10.014 (cit. on p. 6).

[18] J. Uranga et al. "Cross-linking of fish gelatins to develop sustainable films with enhanced properties". In: *European Polymer Journal* 78 (2016-05), pp. 82–90. ISSN: 00143057. DOI: 10.1016/j.eurpolymj.2016.03.017 (cit. on p. 6).

[19] G. Xing et al. "Citric acid crosslinked chitosan/poly(ethylene oxide) composite nanofibers fabricated by electrospinning and thermal treatment for controlled drug release". In: *Cellulose* 28.2 (2021-01), pp. 961–971. ISSN: 1572882X. DOI: 10.1007/s10570-020-03562-3 (cit. on pp. 6, 14).

[20] H. J. Wiggers et al. "Quercetin-Crosslinked Chitosan Films for Controlled Release of Antimicrobial Drugs". In: *Frontiers in Bioengineering and Biotechnology* 10 (2022-03). ISSN: 22964185. DOI: 10.3389/fbioe.2022.814162 (cit. on p. 6).

[21] A. V. Anand David, R. Arulmoli, and S. Parasuraman. "Overviews of biological importance of quercetin: A bioactive flavonoid". In: *Pharmacognosy Reviews* 10.20 (2016-07), pp. 84–89. ISSN: 09762787. DOI: 10.4103/0973-7847.194044 (cit. on p. 7).

[22] A. Chahardoli et al. "Optimization of Quercetin-Assisted Silver Nanoparticles Synthesis and Evaluation of Their Hemocompatibility, Antioxidant, Anti-Inflammatory, and Antibacterial effects". In: *Global Challenges* 5.12 (2021-12). ISSN: 20566646. DOI: 10.1002/gch2.202100075 (cit. on pp. 7, 12, 30).

[23] Y. Wang et al. "Drug delivery based pharmacological enhancement and current insights of quercetin with therapeutic potential against oral diseases". In: *Biomedicine and Pharmacotherapy* 128 (2020-08). ISSN: 19506007. DOI: 10.1016/j.biopha.2020.110372 (cit. on pp. 7, 11).

[24] P. Vashisth, R. P. Singh, and V. Pruthi. "A controlled release system for quercetin from biodegradable poly(lactide-co-glycolide)-polycaprolactone nanofibers and its in vitro antitumor activity". In: *Journal of Bioactive and Compatible Polymers* 31.3 (2016-05), pp. 260–272. ISSN: 15308030. DOI: 10.1177/0883911515613098 (cit. on pp. 7, 21).

[25] H. Choudhury et al. "Silver nanoparticles: Advanced and promising technology in diabetic wound therapy". In: *Materials Science and Engineering C* 112 (2020-07). ISSN: 18730191. DOI: 10.1016/j.msec.2020.110925 (cit. on p. 7).

[26] A. Naganthran et al. "Synthesis, Characterization and Biomedical Application of Silver Nanoparticles". In: *Materials* 15.2 (2022-01). ISSN: 19961944. DOI: 10.3390/ma15020427 (cit. on p. 7).

[27] E. Sánchez-López et al. "Metal-based nanoparticles as antimicrobial agents: An overview". In: *Nanomaterials* 10.2 (2020-02). ISSN: 20794991. DOI: 10.3390/nano10020292 (cit. on p. 8).

[28] C. You et al. "Silver nanoparticle loaded collagen/chitosan scaffolds promote wound healing via regulating fibroblast migration and macrophage activation". In: *Scientific Reports* 7.1 (2017-12). ISSN: 20452322. DOI: 10.1038/s41598-017-10481-0 (cit. on pp. 9, 10).

[29] B. Vafania, M. Fathi, and S. Soleimanian-Zad. "Nanoencapsulation of thyme essential oil in chitosan-gelatin nanofibers by nozzle-less electrospinning and their application to reduce nitrite in sausages". In: *Food and Bioproducts Processing* 116 (2019-07), pp. 240–248. ISSN: 09603085. DOI: 10.1016/j.fbp.2019.06.001 (cit. on p. 9).

[30] S. Ebrahimi, M. Fathi, and M. Kadivar. "Production and characterization of chitosan-gelatin nanofibers by nozzle-less electrospinning and their application to enhance edible film's properties". In: *Food Packaging and Shelf Life* 22 (2019-12). ISSN: 22142894. DOI: 10.1016/j.fpsl.2019.100387 (cit. on p. 9).

[31] S. R. Gomes et al. "In vitro and in vivo evaluation of electrospun nanofibers of PCL, chitosan and gelatin: A comparative study". In: *Materials Science and Engineering C* 46 (2015-01), pp. 348–358. ISSN: 09284931. DOI: 10.1016/j.msec.2014.10.051 (cit. on pp. 9, 37).

[32] S. Gomes et al. "Evaluation of nanofibrous scaffolds obtained from blends of chitosan, gelatin and polycaprolactone for skin tissue engineering". In: *International Journal of Biological Macromolecules* 102 (2017-09), pp. 1174–1185. ISSN: 18790003. DOI: 10.1016/j.ijbiomac.2017.05.004 (cit. on pp. 10, 13, 24).

[33] G. Sabarees et al. "Recent Advances in Silver Nanoparticles Containing Nanofibers for Chronic Wound Management". In: *Polymers* 14.19 (2022-10). ISSN: 20734360. DOI: 10.3390/polym14193994 (cit. on p. 10).

[34] M. Ganesh et al. "Sulfanilamide and silver nanoparticles-loaded polyvinyl alcohol-chitosan composite electrospun nanofibers: Synthesis and evaluation on synergism in wound healing". In: *Journal of Industrial and Engineering Chemistry* 39 (2016-07), pp. 127–135. ISSN: 22345957. DOI: 10.1016/j.jiec.2016.05.021 (cit. on p. 10).

[35] J. Shao et al. "Antibacterial effect and wound healing ability of silver nanoparticles incorporation into chitosan-based nanofibrous membranes". In: *Materials Science and Engineering C* 98 (2019-05), pp. 1053–1063. ISSN: 18730191. DOI: 10.1016/j.msec.2019.01.073 (cit. on p. 10).

[36] R. Goyal et al. "Nanoparticles and nanofibers for topical drug delivery". In: *Journal of Controlled Release* 240 (2016-10), pp. 77–92. ISSN: 18734995. DOI: 10.1016/j.jconrel.2015.10.049 (cit. on p. 11).

[37] F. Mohammadian and A. Eatemadi. "Drug loading and delivery using nanofibers scaffolds". In: *Artificial Cells, Nanomedicine and Biotechnology* 45.5 (2017-07), pp. 881–888. ISSN: 2169141X. DOI: 10.1080/21691401.2016.1185726 (cit. on p. 11).

[38] G. Ajmal et al. "Biomimetic PCL-gelatin based nanofibers loaded with ciprofloxacin hydrochloride and quercetin: A potential antibacterial and anti-oxidant dressing material for accelerated healing of a full thickness wound". In: *International Journal of Pharmaceutics* 567 (2019-08). ISSN: 18733476. DOI: 10.1016/j.ijpharm.2019.118480 (cit. on pp. 11, 21, 25, 36).

[39] A. Choudhary et al. "Quercetin loaded chitosan tripolyphosphate nanoparticles accelerated cutaneous wound healing in Wistar rats". In: *European Journal of Pharmacology* 880 (2020-08). ISSN: 18790712. DOI: 10.1016/j.ejphar.2020.173172 (cit. on p. 11).

[40] L. Zhou et al. "Electrospun chitosan oligosaccharide/polycaprolactone nanofibers loaded with wound-healing compounds of Rutin and Quercetin as antibacterial dressings". In: *International Journal of Biological Macromolecules* 183 (2021-07), pp. 1145–1154. ISSN: 18790003. DOI: 10.1016/j.ijbiomac.2021.05.031 (cit. on pp. 11, 30).

[41] S. K. Karuppannan et al. "Quercetin functionalized hybrid electrospun nanofibers for wound dressing application". In: *Materials Science and Engineering: B* 285 (2022-11). ISSN: 09215107. DOI: 10.1016/j.mseb.2022.115933 (cit. on pp. 11, 21, 28).

[42] R. Badhwar et al. "Quercetin loaded silver nanoparticles in hydrogel matrices for diabetic wound healing". In: *Nanotechnology* 32.50 (2021-12). ISSN: 13616528. DOI: 10.1088/1361-6528/ac2536 (cit. on p. 12).

[43] P. Miguel, C. Ribeiro, and B. In Biochemistry. "Cytotoxicity of Electrospun mats loaded with an-timicrobial agents towards Macrophages". PhD thesis (cit. on p. 13).

[44] A. S. Pádua et al. "Electrospun poly(N-vinylpyrrolidone) membranes with Ag nanoparticles for wound dressings: Production and characterization". In: *Journal of Drug Delivery Science and Technology* 101 (2024-11). ISSN: 17732247. DOI: 10.1016/j.jddst.2024.106303 (cit. on pp. 14, 33).

[45] C. A. Schneider, W. S. Rasband, and K. W. Eliceiri. *NIH Image to ImageJ: 25 years of Image Analysis HHS Public Access*. Tech. rep. 7. 2012, pp. 671–675 (cit. on p. 15).

[46] "Tech Note_ Dynamic Light Scattering_ An Introduction in 30 Minutes". In: *Chemistry, Materials Science* (2005). URL: https://api.semanticscholar.org/CorpusID:11984431 (cit. on p. 15).

[47] P. I. Soares et al. "Iron oxide nanoparticles stabilized with a bilayer of oleic acid for magnetic hyperthermia and MRI applications". In: *Applied Surface Science* 383 (2016-10), pp. 240–247. ISSN: 01694332. DOI: 10.1016/j.apsusc.2016.04.181 (cit. on p. 15).

[48] B. Singh and L. Pal. "Development of sterculia gum based wound dressings for use in drug delivery". In: *European Polymer Journal* 44.10 (2008-10), pp. 3222–3230. ISSN: 00143057. DOI: 10.1016/j.eurpolymj.2008.07.013 (cit. on p. 16).

[49] *"Quest Calculate™ Acetate Buffer (pH 3.6 to 5.6) Preparation and Recipe."* 2024-06 (cit. on p. 16).

[50] Y. Saghafi et al. "Bromelain- and Silver Nanoparticle-Loaded Polycaprolactone/Chitosan Nanofibrous Dressings for Skin Wound Healing". In: *Gels* 9.8 (2023-08). ISSN: 23102861. DOI: 10.3390/gels9080672 (cit. on pp. 21, 36).

[51] S. H. Park and J. C. Kim. "Complexation-responsive monoolein cubic phase containing extract of Bambusae Caulis in Taeniam". In: *International Journal of Polymeric Materials and Polymeric Biomaterials* 69.1 (2020-01), pp. 44–52. ISSN: 1563535X. DOI: 10.1080/00914037.2018.1539986 (cit. on p. 24).

[52] W. S. Vedakumari et al. "Quercetin impregnated chitosan–fibrin composite scaffolds as potential wound dressing materials — Fabrication, characterization and in vivo analysis". In: *European Journal of Pharmaceutical Sciences* 97 (2017-01), pp. 106–112. ISSN: 18790720. DOI: 10.1016/j.ejps.2016.11.012 (cit. on p. 24).

[53] A. S. Bernadette Agu et al. "Synthesis and Characterization of a chitosan-based citric acid crosslinked encapsulant system". In: *J. Chil. Chem. Soc* 64 (2019), p. 4 (cit. on p. 24).

[54] M. Catauro et al. "Silica/quercetin sol-gel hybrids as antioxidant dental implant materials". In: *Science and Technology of Advanced Materials* 16.3 (2015-06). ISSN: 14686996. DOI: 10.1088/1468-6996/16/3/035001 (cit. on p. 25).

[55] S. Ediyilyam et al. "Chitosan/gelatin/silver nanoparticles composites films for biodegradable food packaging applications". In: *Polymers* 13.11 (2021-06). ISSN: 20734360. DOI: 10.3390/polym13111680 (cit. on p. 26).

[56] M. Danaei et al. "Impact of particle size and polydispersity index on the clinical applications of lipidic nanocarrier systems". In: *Pharmaceutics* 10.2 (2018-05). ISSN: 19994923. DOI: 10.3390/pharmaceutics10020057 (cit. on p. 26).

[57] R. Vazquez-Muñoz, N. Bogdanchikova, and A. Huerta-Saquero. "Beyond the Nanomaterials Approach: Influence of Culture Conditions on the Stability and Antimicrobial Activity of Silver Nanoparticles". In: *ACS Omega* 5.44 (2020-11), pp. 28441–28451. ISSN: 24701343. DOI: 10.1021/acsomega.0c02007 (cit. on p. 26).

[58] C. Kong et al. "Riclin-Capped Silver Nanoparticles as an Antibacterial and Anti-Inflammatory Wound Dressing". In: *International Journal of Nanomedicine* 17 (2022), pp. 2629–2641. ISSN: 11782013. DOI: 10.2147/IJN.S366899 (cit. on p. 27).

[59] Z. Babaei et al. "In situ synthesis of gold/silver nanoparticles and polyaniline as buffer layer in polymer solar cells". In: *Materials Chemistry and Physics* 248 (2020-07). ISSN: 02540584. DOI: 10.1016/j.matchemphys.2020.122879 (cit. on p. 27).

[60] C. A. Ferreira et al. "Multifunctional gelatin/chitosan electrospun wound dressing dopped with undaria pinnatifida phlorotannin-enriched extract for skin regeneration". In: *Pharmaceutics* 13.12 (2021-12). ISSN: 19994923. DOI: 10.3390/pharmaceutics13122152 (cit. on pp. 27, 29, 32).

[61] T. P. Pivetta et al. "Topical formulation of quercetin encapsulated in natural lipid nanocarriers: Evaluation of biological properties and phototoxic effect". In: *Journal of Drug Delivery Science and Technology* 53 (2019-10). ISSN: 17732247. DOI: 10.1016/j.jddst.2019.101148 (cit. on p. 28).

[62] C. Ulker Turan and Y. Guvenilir. "Electrospun poly(ω-pentadecalactone-co-ϵ-caprolactone)/gelatin/chitosan ternary nanofibers with antibacterial activity for treatment of skin infections". In: *European Journal of Pharmaceutical Sciences* 170 (2022-03). ISSN: 18790720. DOI: 10.1016/j.ejps.2021.106113 (cit. on p. 28).

[63] W. Zhang et al. "Modeling the primary size effects of citrate-coated silver nanoparticles on their ion release kinetics". In: *Environmental Science and Technology* 45.10 (2011-05), pp. 4422–4428. ISSN: 0013936X. DOI: 10.1021/es104205a (cit. on p. 29).

[64] D. Paneva et al. "Antibacterial electrospun poly(ϵ-caprolactone)/ascorbyl palmitate nanofibrous materials". In: *International Journal of Pharmaceutics* 416.1 (2011-09), pp. 346–355. ISSN: 03785173. DOI: 10.1016/j.ijpharm.2011.06.032 (cit. on p. 30).

[65] B. H. Kim et al. "Relative antioxidant activities of quercetin and its structurally related substances and their effects on NF-κB/CRE/AP-1 signaling in murine macrophages". In: *Molecules and Cells* 35.5 (2013-05), pp. 410–420. ISSN: 10168478. DOI: 10.1007/s10059-013-0031-z (cit. on pp. 30, 34).

[66] L. Da Silva Uebel et al. "Quercetin and curcumin in nanofibers of polycaprolactone and poly(hydroxybutyrate-co-hydroxyvalerate): Assessment of in vitro antioxidant activity". In: *Journal of Applied Polymer Science* 133.30 (2016-08). ISSN: 10974628. DOI: 10.1002/app.43712 (cit. on p. 30).

[67] J. López-García et al. "HaCaT Keratinocytes Response on Antimicrobial Atelocollagen Substrates: Extent of Cytotoxicity, Cell Viability and Proliferation". In: *Journal of Functional Biomaterials* 5.2 (2014-05), pp. 43–57. ISSN: 2079-4983. DOI: 10.3390/jfb5020043 (cit. on p. 31).

[68] *ISO 10993-5:2009(en) Biological evaluation of medical devices — Part 5: Tests for in vitro cytotoxicity*. 2009-06 (cit. on p. 31).

[69] H. A. Rather et al. "Antioxidative study of Cerium Oxide nanoparticle functionalised PCL-Gelatin electrospun fibers for wound healing application". In: *Bioactive Materials* 3.2 (2018-06), pp. 201–211. ISSN: 2452199X. DOI: 10.1016/j.bioactmat.2017.09.006 (cit. on p. 34).

[70] X. Zhu et al. "Protective effects of quercetin on UVB irradiation-induced cytotoxicity through ROS clearance in keratinocyte cells". In: *Oncology Reports* 37.1 (2017-01), pp. 209–218. ISSN: 17912431. DOI: 10.3892/or.2016.5217 (cit. on p. 34).

[71] T. Vieira et al. "Electrospun biodegradable chitosan based-poly(urethane urea) scaffolds for soft tissue engineering". In: *Materials Science and Engineering C* 103 (2019-10). ISSN: 18730191. DOI: 10.1016/j.msec.2019.109819 (cit. on p. 37).

A

SEM-EDS

Figure A.1 refers to the membranes containing AgNPs. For both membranes, CS-GEL + AgNPs and CS-GEL + Quer + AgNPs, there is a visible SEM-EDS figure with only the green marks referring to Ag, and a mixture of all the elements.

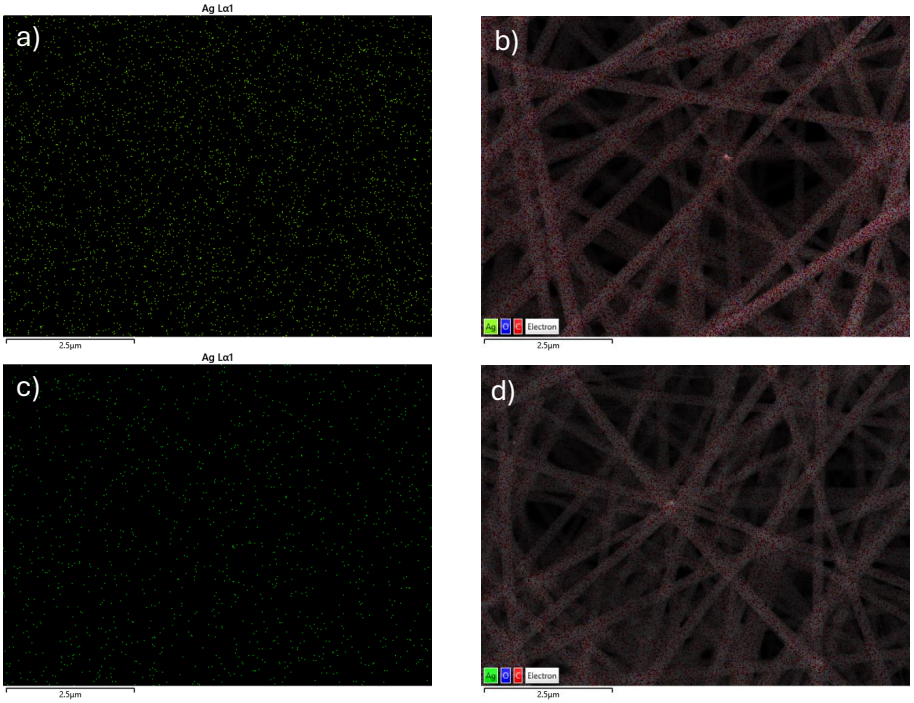

Figure A.1: SEM/EDS images of CS-GEL + AgNPs (top) and CS-GEL + Quer + AgNPs (bottom). The imagens on the left side are reference to atoms of Ag, and the right side to the mix of all the elements. Scale bar: 250 µm.

B

Equations for DLS

To analyze data from dynamic light scattering measurements, the cumulants expansion approach was applied for each experiment as mentioned in the Sections DLS. This method relies on the expansion of the expression that connects the autocorrelation curve with the experimental curve into Taylor series, as described by Equation B.1:

$$C(\tau) = 1 + \beta \exp(-2\Gamma\tau) \tag{B.1}$$

Here, τ represents the delay time (in microseconds), C is the autocorrelation, β is a pre-exponential factor, and Γ is the decay constant, which provides the average value $\langle\tau\rangle$. In a first-order expansion, $\langle\tau\rangle = \Gamma^{-1}$, and:

$$\Gamma = Dq^2 \tag{B.2}$$

In Equation B.2, D is the diffusion coefficient and q is the scattering vector, determined by Equation B.3:

$$q = \frac{4\pi n}{\lambda} \sin\left(\frac{\theta}{2}\right) \tag{B.3}$$

In this equation, n is the refractive index, λ is the wavelength (532 nm), and θ is the scattering angle (90°).

Finally, the hydrodynamic diameter of the samples can be determined using the Stokes-Einstein equation, shown in Equation B.4:

$$D_h = \frac{k_B T}{3\pi\eta(T)D} \tag{B.4}$$

In Equation B.4, k_B represents the Boltzmann constant, T is the absolute temperature, and η denotes the fluid viscosity.

C

In Vitro Protocols

C.1 Culture Protocol

With the aim of perform a cell culture with SHSYS5, HFF2 or HaCat, a similar protocol is followed for each. These cells are seeded in either a T25 or T75 flask until they reach an appropriate confluency. Once this state is achieved, the medium is removed, and the cells are washed with 5 mL or 10 mL of PBS for T25 or T75 flasks, respectively. The cells are then trypsinized with 500 µL or 1 mL of Trypsin (TrypLETM Express, Gibco) for 5 minutes in an incubator. After this period, the cells are resuspended in 5 mL or 10 mL (T25 or T75) of DMEM depending on the cell line: DMEM-Low Glucose for SH-SY5Y and HFFF2 cells, and DMEM-High Glucose for HaCat cells. The medium is supplemented with 5 % heat-inactivated fetal bovine serum (FBS, Biowest) and 1 % penicillin-streptomycin (P/S, Gibco). The cell suspension is then transferred to a Falcon tube. To estimate the number of cells in the cell suspension, 50 µL of trypan blue was mixed with 50 µL of the cell suspension in an eppendorf. This solution was then placed in a hemocytometer to calculate the cell density, expressed as cells/mL. By averaging the counts from 9 squares on the hemocytometer, the cell density was calculated by multiplying this average by the dilution factor (2) and by 10,000, which is the hemocytometer's conversion factor. After determining the cell density in the suspension, the necessary volumes of the suspension and medium are calculated to achieve the required number of cells per well. To determine the total number of cells required, the number of wells was multiplied by the surface area of each well (0.3 cm^2 for 96-well plates and 1 cm^2 for 24-well plates with O-rings), providing the total surface area that needed to be covered. For the 24-well plates, each well is loaded with 500 µL of solution, and for the 96-well plates, 100 µL of solution is required per well. Using these values, along with the cell density of the solution and the area of each well, it is possible to estimate how much of the cell suspension is needed to mix with the medium to achieve the desired seeding for all wells.

C.2 Resazurin Assay Protocol

After the required incubation period for each experiment, the medium in the wells was replaced with an equal volume of resazurin solution. This resazurin solution was prepared by mixing resazurin at a concentration of 0.04 g/mL with DMEM medium in a 1:1 (v/v) ratio. Following a 3-hour incubation, absorbance values were measured using a Biotek 8000UV at two different wavelengths: 600 nm and 570 nm. The resazurin conversion index was calculated by subtracting the absorbance at 600 nm from the absorbance at 570 nm. The controls used for the resazurin assay included: a negative control (c-), representing living cells; a positive control (c+), representing dead cells; and a resazurin control, consisting of the prepared mixture of resazurin and DMEM medium.

D

Calibration Curve

This appendix presents the calibration curve for quercetin, which was used for quantification in this work.

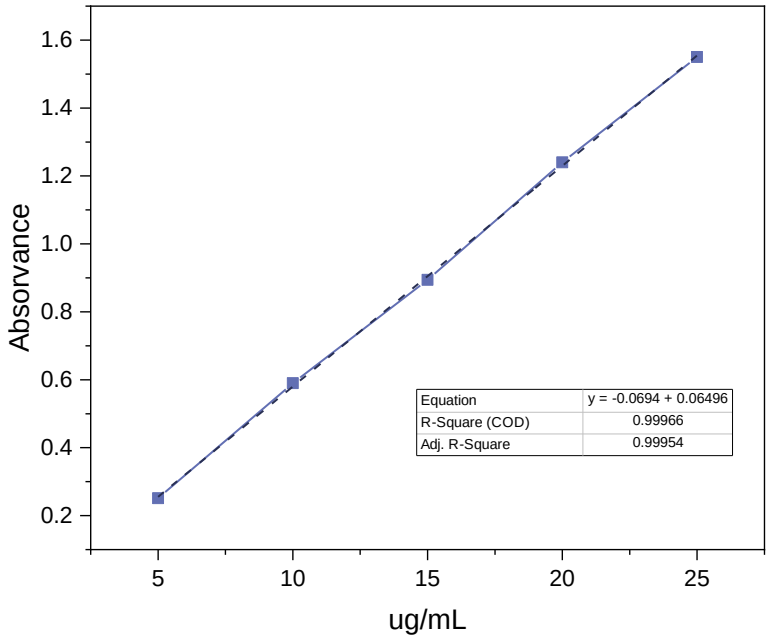

Figure D.1: Calibration curve for quercetin. The curve shows the relationship between absorbance and quercetin concentration, fitted to a linear regression.

E

Cumulative Mass Release Calculation

To determine the cumulative mass release throughout the assay, the absorbance measurements were converted into mass concentration ($\mu g/mL$) using the calibration curve.

At each time point t, the released mass (M_t) was calculated using the Equation E.1:

$$M_t = (C_t \times V_{\text{total}}) - (C_{t-1} \times V_{\text{remaining}}) \tag{E.1}$$

where: C_t is the concentration ($\mu g/mL$) of the analyte at time t; C_{t-1} is the concentration ($\mu g/mL$) at the previous time point ($t-1$); V_{total} = 8 mL is the total volume of the release medium; $V_{\text{remaining}}$ = 6 mL is the volume that remains in the solution after removing 2 mL for measurement.

At each time point, 2 mL of the solution was withdrawn for absorbance measurement and discarded, while 6 mL of the previous solution remained. The 2 mL withdrawn was replaced with fresh buffer to maintain a constant total volume of 8 mL. This means that the analyte present in the remaining 6 mL contributes to the next time point's total, and the calculation must account for this carryover effect.

The cumulative released mass ($M_{\text{cumulative},t}$) was then determined by summing the released mass at the current time point with the previously accumulated mass, as showed in Equation E.2.

$$M_{\text{cumulative},t} = M_{\text{cumulative},t-1} + M_t \tag{E.2}$$

This approach ensures that the progressive release accounts for both the newly released analyte and the residual concentration from the previous time points.